EP300 (p300) mediated histone butyrylation is critical for adipogenesis

Running title: Lysine butyrylation inhibition blocks adipogenesis

Aditya Bhattacharya [1], Sourav Chatterjee [1], Utsa Bhaduri [2], Akash Kumar Singh [1], Koneni V Sashidhara [4], Rajdeep Guha [5], Aamir Nazir [6], Srikanta Kumar Rath [6], Nagashayana Natesh , Tapas K Kundu [1,3]

1 Transcription and Disease Laboratory, Molecular Biology and Genetics Unit, Jawaharlal Nehru Centre for Advanced Scientific Research, Bangalore, India.
2 Chromatin Biology Laboratory, Molecular Biology and Genetics Unit, Jawaharlal Nehru Centre for Advanced Scientific Research, Bangalore, India.
3 Division of Neuroscience and Aging Biology,CSIR-Central Drug Research Institute, Lucknow
4 Division of Medicinal and Process Chemistry, Central Drug Research Institute, Lucknow, India
5 Division of Laboratory Animal Facility, Central Drug Research Institute, Lucknow, India
6 Division of Toxicology and Experimental Medicine, Central Drug Research Institute, Lucknow, India
7 Central Government Health Scheme Wellness Centre Number 8, Domlur, Bangalore, India

E-mail ID of corresponding author: tapas@jncasr.ac.in

Affiliations:

Aditya Bhattacharya – PhD graduate student

Sourav Chatterjee – Post-doctoral researcher

Utsa Bhaduri – Research assistant

Akash Kumar Singh - Integrated PhD student

Koneni V Sashidhara - Professor

Rajdeep Guha – Assistant Professor

Aamir Nazir- Principal Scientist

Srikanta Kumar Rath- Chief Scientist

Nagashayana Natesh – Senior physician

Tapas K Kundu - Professor

Abstract

The master epigenetic enzyme EP300 (p300) besides having lysine acetyltransferase activity can also catalyse other acylation modifications (propionylation, butyrylation, crotonylation etc.), the physiological implications of which are yet to be established fully. Here, by performing immunoblotting and chromatin immunoprecipitation assays, we report that histone butyrylation increases both globally as well as locally in the promoters of pro-adipogenic genes upon adipogenesis. Moreover, the enzyme ACSS2 which is responsible for generating acyl CoA for being used as a cofactor in acylation reactions is upregulated in adipogenesis and its genetic ablation leads to reduction of butyrylation. To delineate the role of p300 catalysed butyrylation from acetylation in adipogenesis, we have identified a semi-synthetic derivative (LTK-14A) of garcinol which specifically inhibited histone butyrylation without affecting acetylation mediated by p300. Treatment of 3T3L1 cells with LTK-14A significantly abolished adipogenesis with downregulation of pro-adipogenic genes along with the inhibition of H4K5 butyrylation. Administering the specific inhibitor to high fat diet fed C57BL6/J mice as well as genetically obese db/db mice led to an attenuation/decrease in their weight gain respectively. The reduced obesity could be at least partially attributed to the targeted inhibition of H4K5 butyrylation, as observed by immunofluorescence staining of the inhibitor treated mice liver sections and immunoblotting with histones extracted from epididymal fat pads. This report therefore not only for the first time causally links histone butyrylation with adipogenesis but also presents a novel small molecule modulator that could be developed for anti-obesity therapeutics. Initial preclinical studies indicate that LTK-14A can be a safe candidate drug for treatment of obesity.

Keywords: Acetylation; adipogenesis; butyrylation; garcinol; p300

50 ## Introduction

51 Chromatin function is spatially and temporally regulated by several processes like incorporation of
52 histone variants, remodeling of nucleosomes by ATP-dependent remodelers and histone post-
53 translational modifications. Interestingly, epigenetics and the metabolic state of the cell are intimately
54 intertwined because the enzymes catalyzing the modifications use co-factors derived from several
55 metabolic reactions (1). In recent times, advancements made in high sensitivity mass spectrometry have
56 led to the discovery of new acylation modifications that structurally resemble acetylation, but differ in
57 hydrocarbon chain length, hydrophobicity and charge (2). Emerging evidence indicates that these
58 modifications occur dynamically on histones and could either have distinct functions from acetylation,
59 or, have a similar but more profound impact on chromatin de-compaction, thereby amplifying the
60 transcriptional output (3). EP300 (p300) is the master acyltransferase that has been found to
61 promiscuously acylate histones using diverse CoA derivatives (2).

62 Due to the rising prevalence of obesity in the modern day society, there has been increased research on
63 the molecular mechanisms behind its manifestation. At the core of obesity lies the adipose tissue which
64 regulates energy homeostasis and metabolism. Hence, the developmental process of adipose tissue i.e.
65 adipogenesis and its dysregulation needs to be studied for clinical management of obesity related
66 disorders. The process of adipogenesis is accompanied by a significant increase in global histone
67 acetylation levels, along with a rise in expression of p300 and a concomitant decrease in the levels of
68 several histone deacetylases (4). Regulation of gene expression is dictated by the fluctuating activities of
69 histone acetyltransferases and histone deacetylases. Moreover, the importance of histone acetylation
70 for adipogenesis has been further underlined by the finding that knockdown of ATP citrate lyase, an
71 enzyme responsible for the regeneration of acetyl CoA in the cytoplasm and nucleus, leads to decrease
72 in histone acetylation and also suppression of adipogenesis (5). Therefore, it can be assumed that p300

73 plays a crucial role in promoting the expression of adipogenesis related genes by acetylating the
74 histones in the corresponding gene regulatory regions, especially the promoters. Amongst the different
75 coenzyme A derivatives, butyric acid is an important short chain fatty acid and an intermediate of fatty
76 acid synthesis/breakdown processes. p300 has been known to carry out butyrylation of histones which
77 has been causally linked to the process of spermatogenesis (3).

78 In this study we report that histone butyrylation is critical in adipoogenesis, probed by the first known
79 acylation specific small molecule inhibitor of p300. The newly discovered importance of histone
80 butyrylation in adipogenesis makes it an attractive target for small molecule compound mediated
81 inhibition of adipogenesis, thereby controlling obesity with lesser collateral damage.

82 **Materials and Methods**

83 **Animals and treatment for obesity related studies:** Male C57BL/6J mice (8 weeks old) were bred in
84 house and acclimatized for 1 week prior to experiments. Mice were maintained on a 12 hour light/dark
85 cycle and given ad libitum access to food and water. Experiments were carried out in accordance with
86 the Committee for the Purpose of Control and Supervision of Experiments on Animals (CPCSEA)
87 guidelines and were approved by the Institutional Animal Ethics Committee of JNCASR
88 (201/GO/Re/S/2000/CPCSEA dated 1st June, 2000 Renewed in Aug 2015). The age-matched animals
89 were maintained on a standard laboratory chow diet (AMRUT M/s Krishna Valley Agrotech ,
90 Maharashtra) or high fat diet (60 kcal% fat) (Research Diets, Cat. No. D12492) with or without LTK-14A
91 (50 mg/Kg body weight) and water. The compound was mixed with the high fat diet according to dosage
92 requirements in the laboratory every week. Body weight and food intake was measured twice every
93 week.

94 For the experiment on genetically obese mice, male db/db mice and db+/- mice (8-10 weeks old) bred in
95 house were obtained and acclimatized for 1 week prior to experiments. Mice were maintained on a 12-

96 hour light/dark cycle at 22+/-3 ℃ and a relative humidity of 55% and given ad libitum access to food and
97 water. The experiments were carried out in accordance with the Committee for the Purpose of Control
98 and Supervision of Experiments on Animals (CPCSEA) guidelines, Government of India and was approved
99 by the Institutional Animal Ethics Committee of CSIR-CDRI, Lucknow (IAEC/2020/115/Renew-
100 0/Sl.No.09). The age-matched animals were maintained on a standard laboratory pelleted diet (Altromin
101 International, Cat. No. 1320) and water. db/db mice were oral gavaged (50 mg/kg) with LTK14A in 0.5%
102 carboxymethyl cellulose, equal volume of the vehicle was orally gavaged to control db/db mice for a
103 total period of 30 days. db+/- animals were kept as untreated normal control group. The body weights
104 and feed intake was recorded every week throughout the experimental period. The lean and fat mass of
105 the mice were determined using Echo MRI in live mice on day 15th and day 30th.
106
107 **Cell culture:** The mammalian cell line 3T3L1 was obtained from ATCC (American Type Culture Collection)
108 and was grown in DMEM (Dulbecco's Modified Eagle's Medium). The growth medium was
109 supplemented with 10% FBS (Fetal Bovine Serum). The cell line was grown in 37°C incubator with 5%
110 CO2 and 90% relative humidity.
111
112 **siRNA experiments:** ON-TARGETplus siRNA SMART pools against mouse Acss2 (catalog no.L-065412-01-
113 0005) was purchased from Dharmacon (Dharmacon, Lafayette, CO, USA). 3T3L1 cells were transfected
114 with Acss2 siRNA at 25 nM concentration, using RNAiMAX (catalog no. 13778-150, Thermo Fisher
115 Scientific) according to manufacturer's protocols. Transfection was carried out for 48 hours after which
116 cells were induced for differentiation for 6 days followed by RNA isolation and histone extraction.
117
118 **Adipogenesis and Oil Red-O staining:** 3T3L1 preadipocytes were grown to confluency and 24 hours
119 post-confluence, cells were incubated with differentiation medium (growth medium containing 1µM

120 Dexamethasone, 0.5 mM IBMX and 1 µg/ml insulin)(Sigma Aldrich) for 2 days in the presence/absence
121 of LTK-14A. Then the cells were supplemented with maintenance medium with/without LTK-14A
122 (growth medium with 1 µg/ml insulin only) every alternate day. On the 6th day post induction of
123 differentiation the cells were fixed with 3.7% formaldehyde solution followed by staining with Oil Red-O
124 dye (Sigma-Aldrich) (prepared in 60% isopropanol) for 1 hour at room temperature. The incorporated
125 dye was extracted using isopropanol and absorbance values were determined spectrophotometrically at
126 510 nm to estimate total amount of lipid accumulation under different experimental conditions.
127
128 **Acid extraction of histones and immunoblotting:** 3T3L1 cells were washed with ice-cold PBS and then
129 resuspended in Triton extraction buffer (PBS containing 0.5% Triton X-100 (v/v) and 2 mM PMSF). The
130 cells were allowed to lyse on ice for 10 minutes, spun down, washed with PBS and the process was
131 repeated another time. Then the proteins were acid extracted with 0.2 N HCl for two hours on ice. The
132 debris was spun down and then histones were precipitated by incubating the supernatant with 33%
133 trichloroacetic acid (Sigma-Aldrich) at 4°C for 30 minutes. The histones were then pelleted down and
134 then given two washes with acetone. The pellet was allowed to air-dry for 10 minutes and then
135 resuspended with 50 mM Tris-Cl, pH 7.4. Extraction of histones from epididymal fat pads was
136 performed by mechanically homogenizing the adipose tissues in Triton extraction buffer and then
137 following the same subsequent steps as mentioned before, except for the step of acid extraction with
138 HCl, in which the incubation was performed for four hours on ice.

139 The samples were then run in 15% SDS-PAGE, transferred onto PVDF membrane (Milipore) in transfer
140 buffer (25 mM Tris, 192 mM glycine, 0.036% SDS in 20% methanol), blocked with 5% skimmed milk
141 solution to prevent non-specific antibody binding and finally probed with antibodies against acetylation
142 and butyrylation marks prepared in 1% skimmed milk or FBS solution (5% BSA, 1x TBS, 0.1% Tween-20).
143 HRP-conjugated secondary antibodies (Abcam) were used against the primary antibodies to obtain a

144 chemiluminiscent signal in the presence of SuperSignal West Pico Chemiluminiscent Substrate (Thermo
145 Scientific) which was developed using the VersaDoc imaging system (Biorad).

146

147 **Synthesis of LTK14A:** Isolation of garcinol from Garcinia indica and synthesis of isogarcinol from it were
148 carried out following the protocols as mentioned in Mantelingu et al, (2007) (11). For LTK-14A synthesis,
149 anhydrous potassium carbonate (0.41 mmol) was added to a stirred solution of isogarcinol (100 mg, 0.16
150 mmol) in dry acetone. The mixture was stirred for 1 hour at room temperature followed by dropwise
151 addition of dimethyl sulfate (0.41 mmol) under nitrogen gas atmosphere. The resulting reaction mixture
152 was further stirred at room temperature for 14 hours. Progress of the reaction was monitored through
153 thin layer chromatography. Acetone was evaporated from the reaction mass, ice was added and
154 acidified with 5% aqueous HCl (pH ~ 5-6). A pale brown precipitate was observed, which was filtered and
155 washed with cold water. The dry mass was then chromatographed on silica gel using 5-6% ethyl acetate
156 in hexane as eluting solvent mixture. 720 mg (69%) LTK14A was isolated as white solid. NMR spectral
157 analysis was consistent with the desired product (Sup. Fig. 3A). A 20 mg sample was dissolved in hot
158 methanol and placed in a flat surface glass vial with access to very slow solvent evaporation. Crystals as
159 colorless needles were isolated. The purity of the synthesized LTK-14A was found to be more than 98%
160 as verified by HPLC (Sup. Fig. 3C) and only the protonated species of LTK-14A were observed in the ESI
161 spectra of the corresponding fraction (Sup. Fig. 3B).

162

163 **X-ray crystal structure determination for LTK14A (CCDC: 1969185):** Suitable single crystal with
164 approximate dimensions of 0.35 × 0.18 × 0.15 mm3 was used for X-ray diffraction analyses by mounting
165 on the tip of a glass fibre in air. Data were collected on a Bruker kappa apex 2 with Mo Kα (λ=0.71073 Å)
166 at 296 (2) K. The structure was solved by direct method using program SHELXL-97 and subsequent Fast

167 Fourier Transform technique. Crystallographic data and experimental details for LTK14A are summarized
168 in Table 1 and Sup. Fig. 3D.

169

170 **Untargeted analysis of intracellular metabolites by Ultra-performance liquid chromatography coupled**
171 **with time-of-flight mass spectrometer (Q-TOF LC/MS):** Profiling of intracellular metabolites was
172 performed on an agilent 1290 Infinity LC system coupled to Agilent 6545 Accurate-Mass Quadrupole
173 Time-of- Flight (QTOF) with Agilent Jet Stream Thermal Gradient Technology. The UPLC system was
174 assembled with a Diode array detector (DAD) and autosampler. The Chromatographic separation was
175 achieved on Agilent ZORBAX SB- C18 column (2.1 × 100 mm, 1.8 µm) as stationary phase. The mobile
176 phase consisted of a linear gradient of 100 mM ammonium formate (A) and Acetonitrile (B): 0–10.0 min,
177 30-80% B (v/v); 10.0–15.0 min, 80–100% B (v/v); 15.0–20.0 min, 100% B (v/v); 20.0–21.0 min, 100–30%
178 B (v/v); 21.0–25.0 min, 30% B. The sample was dissolved in 1 ml methanol (LCMS Grade), centrifuged
179 and supernatant was taken for UPLC-QTOF-MS analysis. The column was reconditioned for 5 minutes
180 prior to the next injection. The flow rate was 0.5 ml/min, and the injected volume was 20 µL. The UPLC
181 was connected to the MS analysis was performed on an Agilent 6545 Accurate-Mass Q-TOF/MS system
182 with an electrospray ionization (ESI) source. Considering the MS conditions, positive ion mode was used
183 to obtain high-resolution mass spectra. The ESI source parameters were: drying gas (N2) flow, 8 L/min;
184 drying gas temperature, 200°C. Other parameters were set as nebuliser gas, 35 psig; capillary voltage,
185 3000 V; skimmer voltage, 65 V; nozzle voltage 1000 V and fragmentor voltage 150 V. The data
186 acquisition on the LC-QTOF was performed using Agilent Mass Hunter Acquisition software (Agilent
187 Technologies, Santa Clara, CA, USA). The data were deconvoluted into individual chemical peaks with
188 Agilent MassHunter Qualitative Analysis (MassHunterQual, Agilent Technologies).

189 **Site directed mutagenesis:** Point mutation was introduced into the p300 catalytic domain sequence
190 cloned within pET-28b plasmid by using the Quikchange site directed mutagenesis kit (Agilent). Briefly,
191 the template was mixed with Pfuturbo DNA polymerase, designed forward and reverse primers and
192 dNTPs for PCR (Initial denaturation for 30 seconds at 95°C; Cycles: 95°C 30'', 55°C for 60'', 68°C for 7';
193 final elongation at 68°C for 5'.) The mixture was then incubated with DpnI enzyme for 2.5 hours for
194 removal of the parent wild type sequence followed by transformation of competent XL10Gold cells and
195 kanamycin selection of positive transformants. The inserted mutation was verified by sequencing and
196 alignment with the wild type sequence using ClustalOmega software. The sequences of the primers used
197 are as follows:

198 Forward primer- 5'- CCTCACTTGGTGGAGCTGCCCAAAATATGCCCTGTTGTG – 3'

199 Reverse primer- 5'- CACAACAGGGCATATTTGGGCAGCTCCACCAAGTGAGG -3'

200

201 **Purification of recombinant full-length p300 and p300 catalytic domain**: Polyhistidine tagged
202 recombinant p300 was purified from Sf21 insect cells by Ni-NTA based affinity chromatography. These
203 cells were infected by the baculovirus containing p300 for 72 hours. Once the cells showed signs of
204 infection, they were scraped off and centrifuged to separate the spent media. The cell pellets were
205 resuspended in ice cold homogenisation buffer (20 mM Tris, pH 7.5; 20 mM imidazole, 10% glycerol, 0.2
206 mM EDTA, 300 mM KCl, 0.1%NP-40, 2 mM PMSF, 2 mM βmercaptoethanol) and then homogenised
207 using a Dounce homogeniser (5 cycles, 6 strokes per cycle with 5 minutes interval between each cycle).
208 The cell debris was separated by centrifugation and then the lysate was incubated with pre-equilibriated
209 Ni-NTA slurry for 2.5 hours at 4°C on an end-to-end rotor. Then the beads were washed with wash
210 buffer (20 mM Tris, pH 7.5; 40 mM imidazole) nine times to remove unwanted contaminants. Finally
211 p300 was eluted using elution buffer (20 mM Tris, pH 7.5; 250 mM imidazole).

212 Polyhistidine tagged p300 catalytic domain cloned in pET28b plasmid and Sirt2 were used for co-
213 transforming BL21(DE3) cells. At first, 50 ml primary culture was prepared in Luria broth containing
214 kanamycin (50 µg/ml) and ampicillin (100 µg/ml) (HIMEDIA) and then it was scaled up 10 times to
215 prepare secondary culture. Incubation was done at 37°C, 180 rpm till O.D. reached 0.37 followed by
216 induction with 0.2 mM IPTG and a further incubation at 30°C for 4 hours. Cells were pelleted at 6000
217 rpm, 4°C for 10 minutes and stored at -80°C. Resuspension and homogenisation of the pellet was
218 carried out in homogenisation buffer (20 mM Tris, pH 7.5; 20 mM imidazole, 10% glycerol, 0.2 mM
219 EDTA, 300 mM KCl, 0.1%NP-40, 2 mM PMSF, 2 mM βmercaptoethanol). 3 cycles of sonication were done
220 for 3 minutes at 35% amplitude with 5 minutes interval between each cycle. The cell debris were
221 separated by pelleting at 12000 rpm for 30 minutes at 4°C. The supernatant was equilibriated with Ni-
222 NTA beads slurry (Novagen) in an end-to-end rotor for 3 hours at 4 C. Eight washes were given with
223 wash buffer (20 mM Tris, pH 7.5; 40 mM imidazole). Elution was carried out in batches with elution
224 buffer (20 mM Tris, pH 7.5; 250 mM imidazole).

225 The enzymatic activity of the proteins was estimated by filter binding assay.

226

227 ***In vitro* filter binding assay:** Different dilutions of purified enzyme were incubated in reaction buffer (50
228 mM Tris-HCl pH 7.5, 1 mM DTT, 10 % Glycerol, 2 mM PMSF) with 10 mM NaBu, tritiated acetyl CoA (50
229 µCi) (PerkinElmer, Part No: NET290050UC) and Xenopus histone H3 (500 ng) for 30 minutes at 30°C. The
230 reaction mixture was then spotted on P81 filter paper and the paper was allowed to dry at room
231 temperature. The paper was washed in wash buffer (50 mM sodium bicarbonate and 50 mM sodium
232 carbonate), dried at 90°C and immersed in enhancing solution (2.5% PPO and 0.25% POPOP in toluene)
233 for taking radioactive counts using liquid scintillation counter (Perkin Elmer, MicroBeta2 system).

234

235 ***In vitro* acylation (acetylation/butyrylation) assay**: Acylation reactions were performed in reaction
236 buffer (25 mM Tris-HCl pH 7.5, 100 mM NaCl, 0.1 mM EDTA, 1 mM DTT, 10 % Glycerol, 1x PIC) with 100
237 ng/mL TSA, and 50 µM Butyryl-CoA/Acetyl CoA. Xenopus histone H3 (1 µg) was used as the substrate
238 and full length p300 or p300 catalytic domain (10,000 cpm activity) was used as the enzyme. Reactions
239 were incubated in presence or absence of butyrylation inhibitor for 10 minutes at 30 °C, followed by
240 initiation of the acetylation/butyrylation reaction by the addition of acetyl CoA/butyryl CoA. After a
241 further 10 minutes, reactions were stopped by addition of Laemmli buffer and samples were used for
242 immunoblotting.

243

244 **Molecular docking analysis:** Glide module of Schrodinger suite was used to dock LTK-14 and LTK-14A to
245 p300 catalytic domain (PDB: 3BIY). Chimera was used as visualizing software. The protein was prepared
246 using the wizard tool in Maestro version 10.2.The crystal structure of LTK-14A (CCDC 1969185) and LTK-
247 14 (CCDC 645420) were used as the most optimized and energy minimized ligand structures. The
248 receptor grid for p300 catalytic domain was generated by specifying the binding (active) site residues
249 using Receptor grid generation in the Schrodinger Glide application. Once the receptor grid was
250 generated, the ligands LTK-14 and LTK-14A were docked to the p300 catalytic domain using Glide
251 version 5.8 molecular docking.

252

253 **Chromatin Immunoprecipitation:** Nuclear ChIP was performed using intact nuclei from cells after
254 removal of lipids. 3T3L1 that were either undifferentiated or differentiated for 3 to 6 days were cross-
255 linked using 1% formaldehyde. Nuclear fractions were obtained by sequentially lysing the cells in two
256 buffers- lysis buffer 1 (140 mM NaCl, 1 mM EDTA, 50 mM HEPES, 10% Glycerol, 0.5% NP-40, 0.25%
257 Triton X-100) and lysis buffer 2 (10 mM Tris pH 8, 200 mM NaCl, 1 mM EDTA, 0.5 mM EGTA). This was

258 followed by lysis in SDS lysis buffer (1% SDS, 10 mM EDTA, 50 mM Tris-HCl pH 8). Lysates were
259 sonicated in a Diagenode Bioruptor (Liège, Belgium) to produce 200 to 1000 bp DNA fragments. The cell
260 lysates were incubated with H4K5 Bu antibody (PTM Biolabs) or preimmune IgG per sample and 25 µl of
261 magnetic protein G Dynabeads (catalog no. 10003D; Novex, Waltham, MA) overnight at 4°C. Beads were
262 then washed successively with low-salt buffer (0.1% SDS, 1% Triton X-100, 2 mM EDTA, 20 mM Tris-HCl
263 pH 8, and 150 mM NaCl), high-salt buffer (0.1% SDS, 1% Triton X-100, 2 mM EDTA, 20 mM Tris-HCl pH
264 8, and 500 mM NaCl), LiCl buffer (250 mM LiCl, 1% NP-40, 1% NaDOC, 1 mM EDTA, and 10 mM Tris-
265 HCl, pH 8), and TE (10 mM Tris-HCl pH 8 and 1 mM EDTA). DNA-protein complexes were recovered
266 from beads in elution buffer (0.1% SDS and 100 mM NaHCO3). The ChIP eluates and input samples in
267 the elution buffer were then reverse cross-linked by adding 200 mM NaCl and 20 µg proteinase K
268 (Sigma) and incubating at 65°C for 4 h. Subsequently, 20 µg of RNase A (Sigma) were added and the
269 samples were further incubated for 15 min at 37°C. The immunoprecipitated DNA was extracted using
270 phenol-chloroform, ethanol precipitated, and used for quantitative PCR. The region-specific primer sets
271 used for the ChIP-qPCR analysis have been mentioned in Table 3. These primers were designed based on
272 the genomic coordinates with enriched H3K27 acetylation in the vicinity of promoters of candidate
273 genes in brown adipose tissue, the information for which was obtained from NCBI37/mm9 assembly
274 (ENCODE/LICR).

275 **Quantitative real time PCR:** Total RNA was isolated from the 3T3L1 cells and epididymal fat pads by
276 phenol-chloroform method. In case of LTK-14A treatment, 3T3L1 cells were allowed to differentiate for
277 7 days following the standard adipogenesis protocol, in presence of the compound at 25 µM
278 concentration. The control experiments were 3T3L1 cells differentiated with or without DMSO as
279 solvent control and differentiation was done only with the addition of only the cocktail of chemicals for
280 adipogenesis. RNA was isolated from the cells after the period of 7 days in all three cases. For isolation
281 of RNA from mice fat pads, the adiose tissue samples were lysed in Trizol using a mechanical

282 homogenizer followed by phenol-chloroform method of extraction. The isolated RNA samples were
283 treated with 2 units/µL DNase I to remove any residual DNA followed by ethanol precipitation at -80°C.
284 2µg RNA was used for cDNA synthesis using MMLV reverse transcriptase (Sigma) in presence of 0.5 mM
285 dNTP and 3.5 µM oligo dT (Sigma). RT-qPCR amplification was done in kappa SYBR green reagent
286 (Biosystems) with the help of Real time PCR instrument (Applied Biosystems by Life Technologies).For
287 estimation of relative fold change in RNA expression, the following calculation was done: Relative fold
288 change = $2^{-\Delta\Delta Ct}$, where ΔΔCt=ΔCt value of sample – ΔCt value of control and ΔCt= Ct value of target – Ct
289 value of internal control actin for individual sample. The sequences of primers are provided in Table 4.

290

291 **Transcriptomics analysis by RNA-seq:** RNA integrity was checked by Agilent Bioanalyzer 2100, only
292 samples with clean rRNA peaks were used. Libraries for RNA-seq were prepared according to KAPA
293 Stranded RNA-Seq Kit with RiboErase (KAPA Biosystems, Wilmington, MA) system. Final library quality
294 and quantity were analyzed by Agilent Bioanalyzer 2100 and Life Technologies Qubit3.0 Fluorometer,
295 respectively. 150 bp Paired-end sequencing was performed on Illumina HiSeq 4000 (Illumnia Inc., San
296 Diego, CA).

297 House mouse (Mus musculus, strain C57BL/6J) genome (mm10) was downloaded from GENCODE and
298 indexed using Bowtie2-build with default parameters. Adapter removal was done using Trim Galore (v
299 0.4.4) and each of the raw Fastq files were passed through a quality check using FastQC. PCR duplicates
300 were removed using the Samtools 1.3.1 with the help of 'rmdup' option. Each of the raw files was then
301 aligned to mm10 genome assembly using TopHat2 with default parameters for paired-end sequencing
302 as described in (28). After aligning, quantification of transcripts was performed using Cufflinks and then
303 Cuffmerge was used to create merged transcriptome annotation. Finally differentially expressed (DE)

304 genes were identified using Cuffdiff. The threshold for DE genes was log2 (fold change) >1.5 for up
305 regulated genes and log2 (fold change) <1.5 for down regulated genes with p-value <0.05.

306 GO enrichment analysis

307 Gene Ontology (GO) analysis was performed in PANTHER (29). Significant enrichment test was
308 performed with the set of differentially expressed genes in PANTHER and Bonferroni correction method
309 was applied to get the best result of significantly enriched biological processes.

310 Fisher's exact test

311 Fisher's exact test was performed in PANTHER Gene Ontology (GO) where p-value significance was
312 calculated based on the ratio of obtained number of genes to the expected number of genes (O/E)
313 considering the total number of genes for the respective pathway in Mus musculus with a FDR of <0.05.

314 Heatmap and clustering of genes

315 Unsupervised hierarchical clustering method was performed using Cluster 3.0 (30) with Pearson
316 Correlation and average linkage rule. Gene expression data (FPKM of all samples) was taken and log2
317 transformed. Low expressed (FPKM<0.05) and invariant genes were removed. Then genes were
318 centered and clustering was performed based on differential expression pattern of genes and fold
319 change. Finally, the heatmap was visualized in Java TreeView 3.0.

320 Biological analysis of differentially expressed transcripts and pathway regulatory network modeling

321 Statistically significant differentially expressed transcripts were subjected to GO and Pathway
322 enrichment using DAVID tool. Only those GO and pathways with a FDR score of <=0.05 was considered
323 for further downstream analysis. Key biologically dysregulated GO and Pathways along with the
324 differentially expressed genes was provided as an input to Pathreg algorithm from Theomics

325 International Pvt Ltd, Bangalore, India for gene regulatory network modeling. The result (nodes and
326 edges) of the Pathreg algorithm was provided as an input to Cytoscape v2.8.2 to identify key nodes and
327 edges that could be representative of the gene regulatory changes upon treatment.

328

329 **Hematoxylin and eosin staining of liver and adipose tissues:** Staining was performed on paraffin
330 embedded sections of liver and epididymal fat pads having the thickness of 5 µm and 10 µm
331 respectively. Briefly, the sections were deparaffinized in xylene, followed by immersion in absolute
332 alcohol, 90% ethanol, 70% ethanol, 50% ethanol and water before staining with hematoxylin for 5-10
333 minutes. The sections were immersed in above mentioned solutions in reverse order before counter-
334 staining in eosin for 15 seconds. Then the samples were dipped in absolute ethanol and xylene before
335 mounting with DPX.

336

337 **Immunohistochemistry:** Collected liver tissue samples were stored in 4% paraformaldehyde for 24
338 hours after which they were cryoprotected in 30% sucrose solution for two weeks. Cryosections were
339 performed at 7 µm sections using Cryostat LeicaCM1850 UV. For staining, the tissue sections were
340 washed with PBS followed by antigen retrieval with 0.01 M citrate buffer (pH 6). The tissues were then
341 permeabilised with 0.3% Triton X-100/PBS (PBST) and blocked with 2% serum followed by incubation
342 with primary antibodies overnight at 4°C. The next day, secondary antibody incubation was carried out
343 for one hour at room temperature followed by staining of the nuclei with Hoechst 33342 and mounting
344 with 70% glycerol. Images were acquired by confocal microscopy. For quantitation, intensity of each
345 modification specific staining was normalized with respect to the Hoechst staining intensity.

346 **MTT assay:** 12500 cells/ml were seeded in presence/absence of LTK-14A in 96-well plate and at
347 different intervals of time (2 days, 4 days, 6 days) , 1/10th volume of 5mg/ml MTT solution was added to
348 it followed by incubation at 37 °C for 3 hours. The formed crystals were dissolved in DMSO and
349 spectrometric estimation of colour intensity was done at 570 nm.

350

351 **Evaluation of mutagenecity by plate incorporation assay:** Five doses of LTK-14A (10.0µg,
352 33.0µg, 100.0µg, 333.0µg and 1000.0µg/plate) were selected to check for its possible
353 mutagenecity. Seven groups decided as Group 1- Control, Group 2 Positive Control and 5 doses
354 of LTK-14A (Group 3 to Group 7: 10.0µg, 33.0µg, 100.0µg, 333.0µg and 1000.0µg/plate) were
355 tested. Four tester strains of *Salmonella typhimurium* (TE 97a, TA 98, TA 100, TA102) were used
356 and their respective positive controls were used in absence of S9 fraction (Table 5); 2-
357 aminoanthracene was used as the positive control in presence of S9 fraction (Table 5). The
358 tester strains were grown overnight in Luria Broth antibiotic selection medium at 37°C. LTK-14A
359 prepared in DMSO was mixed with the bacterial culture, 0.5mM Histidine-Biotin and top agar in
360 a culture tube and the content was overlaid on to minimal glucose plate. In case of plate
361 incorporation assay with S9 mix, LTK-14A was incubated with S9 mix in cold condition for 15 to
362 20 minutes followed by the same procedure as the plate incorporation assay without S9. The
363 plates were incubated in an inverted position in 37°C incubators for 48 hours following which
364 the number of revertants was counted using automated colony counter.

365 **Single dose toxicity study:** The single dose toxicity study on LTK-14A was conducted in accordance with
366 Good Laboratory Practice Principles as published by the OECD in 1998, in accordance with the Drugs and
367 Cosmetics Rule (New Drugs and Clinical trials, 2019/ DCGI). LTK-14A (formulated in vehicle i.e. 0.5%

368 sodium salt of carboxymethyl cellulose) was administered to Sprague Dawley rats once by oral route on
369 the day of scheduled treatment. The three treatment groups were 250 mg, 500 mg, and 1000 mg/kg
370 body weight, while vehicle control was administered to control group. The rat equivalent doses were
371 calculated from the dosage used in mice experiments following FDA guidelines for drug administration.
372 The doses finally administered were 10, 20 and 40 times the corresponding mice equivalent dose. Food,
373 but not water, was removed thus letting the animals fast over night prior to dosing. After administration
374 of LTK-14A, food was withheld for further 2-3 hours and the animals were observed at 30 minutes, 1
375 hour, 2 hours and 4 hours from the time of dosing. Animals were subsequently observed once daily for
376 any signs of toxicity, mortality, or any other observations including conditions of skin, hair coat, eyes,
377 mucous membrane, movement, activity, tremors, convulsions, salivation, diarrhea, posture, piloerection
378 and lethargy. Food intake, water intake and body weight of animals was recorded weekly. Terminal
379 sacrifice of surviving animals was performed after 14 days using CO2 euthanasia technique following
380 which animals were necropsied. Animals were fasted over night before necropsy. Gross observations
381 were recorded.
382

383 **Reagents and antibodies:** The media used for cell culture was purchased from Sigma-Aldrich; DMEM
384 (Ref: 1152). Several other cell culture reagents were obtained from HIMEDIA, such as PBS (Ref: TL1006),
385 Trypsin-EDTA solution 10X (Ref: TCL070) and Antibiotic antimyotic solution 100X (Ref: A002A). Multiple
386 reagents used for cell culture were obtained from Sigma-Aldrich: Insulin (Ref: I6634), Dexamethasone
387 (Ref: D4902), IBMX (Ref: I5879). TRIzol reagent was obtained from ambion life technologies (Ref:
388 15596018). The commercial antibodies used in this study are Pan anti-butyryllysine (PTM Biolabs, SKU:
389 PTM 301), Butyryl-Histone H4 (Lys 12) rabbit pAb (PTM Biolabs, SKU: PTM 308), Butyryl-Histone H3 (Lys
390 9) rabbit pAb (PTM Biolabs, SKU: PTM 305), Butyryl-Histone H3 (Lys 23) mouse mAb (PTM Biolabs, SKU:
391 PTM 307), Butyryl-Histone H4 (Lys 8) rabbit pAb (PTM Biolabs, SKU: PTM 311), Butyryl-Histone H4 (Lys 5)

392 rabbit pAb (PTM Biolabs, SKU: PTM 313), Butyryl-Histone H3 (Lys 27) rabbit pAb (PTM Biolabs, SKU: PTM
393 315).

394 **Statistical analysis:** All statistical analyses were performed using GraphPad Prism 7 Software (California,
395 USA). Data obtained from two or three individual experiments as mentioned in figure legends, were
396 expressed as mean +/- SD. Either two-tailed unpaired Student's t-test or one-way ANOVA with
397 Dunnett's/Bonferroni's multiple comparision was used to determine the statistical significance values.

398 The mutagenecity analysis data was analyzed by comparing the groups using One-way ANOVA followed
399 by Neman-Keuls test. Body weight data for acute toxicity test were summarized in Mean ± SD and
400 compared by two factor (Group and Period) repeated measure analysis of variance (RM ANOVA) and the
401 significance of mean difference within (intra) and between (inter) the groups was done by Newman-
402 Keuls post hoc test. A P-value of equal to or less than 0.05 was considered statistically significant.

403 **Acknowledgements:** TKK is a recipient of JC Bose fellowship from Dept. of Science and Technology,
404 Govt. of India (SR/S2/JCB-28/2010). AB is a senior research fellow of UGC. This work was supported by
405 Life Science Education & Training at JNCASR grant (DBT/INF/22/SP27679/2018). We acknowledge Dr.
406 Rahul Gajbhiye from NIPER, Kolkata for the assistance in mass spectrometry related experiments in their
407 central instrument facility. We thank Dr. R.G. Prakash for providing the necessary facilities to perform
408 the mice experiment in Animal Facility, JNCASR and the confocal facility, JNCASR for the
409 immunofluorescence imaging analysis. We also thank Kruthi HT for helping in preparation of the figures
410 and graphical abstract. We further acknowledge the Sophisticated Analytical Instrument Facility and
411 Research (SAIFR, Lucknow) for providing spectral data. This manuscript bears CDRI communication
412 number 2021/TK.

413

414 **Conflict of interest:** Authors declare no conflict of interest.

415 **Author Contributions:** AB and TKK conceived the project. AB designed and performed all the biological
416 experiments. SC performed initial synthesis of all compounds and molecular docking analysis. KVS
417 performed bulk scale synthesis of LTK-14A for animal experiments. AKS and RG assisted in the animal
418 experiments. UB performed *in silico* analysis of high throughput RNA sequencing data. AN did the
419 toxicity evaluation and SKR evaluated the mutagenecity. NN provided the raw material *Garcinia indica*
420 for compound isolation. AB and TKK analyzed the data and wrote the manuscript.

421 **Results**

422 **Physiological levels of butyryl CoA and histone butyrylation increases during adipogenesis:**

423 Under normal circumstances, the cellular levels of specific coenzyme A derivatives are much less than
424 acetyl CoA (6).We surmised that the situation might alter in particular cases where metabolic pathways
425 promoting the production of other acyl CoA derivatives become more predominant. One such possible
426 scenario could be the process of adipogenesis in which fatty acid synthesis and breakdown can give rise
427 to several intermediate products like butyryl CoA.

428 The causal relationship of butyryl CoA and adipogenesis was investigated using 3T3L1 pre-adipocyte cell
429 line as model system (fig 1A). Our RT-qPCR data showed a significant increase in the expression of *Acss2*
430 (acyl-CoA synthetase short-chain family member 2) upon differentiation (fig 1B). Previously, ACSS2 had
431 been established as the enzyme responsible for generation of acyl-CoA derivatives from their
432 corresponding short chain fatty acids (7). Indeed, siRNA mediated knockdown of *Acss2* (fig 1C) led to a
433 drastic reduction in histone butyrylation with relatively lesser effect on acetylation (fig 1D). This
434 indicated that the ACSS2 generated butyryl CoA might be playing an important physiological role in
435 adipogenesis. These findings prompted us to investigate whether adipocyte differentiation also led to an

436 increased butyrylation of proteins. We observed that in accordance with the previous report (4), there
437 was an increase in acetylation level at histone H3 lysine 9 (H3K9 Ac) in the differentiated cells as
438 compared to the undifferentiated cells (Fig. 1C, panel i). Interestingly immunoblotting with pan
439 butyryllysine and site specific antibodies (H3K9, H3K23, H3K27, H4K5, H4K8 and H4K12) against
440 butyrylation (Fig 1C, panel ii and iii) revealed that butyrylation at each of these sites also increased upon
441 differentiation. Chromatin immunoprecipitation with antibody against H4K5 butyrylation revealed that
442 the modification enrichment levels increased in promoters of different pro-adipogenic genes in a time
443 dependant manner. *Pparg*, the master regulator of adipogenesis, exhibited a steady increase in
444 butyrylation level in its promoter with the progress of differentiation (fig 1F, panel i) while butyrylation
445 increased only at the terminal stage of adipogenesis in the promoter of *Lep*, encoding the adipocyte
446 marker leptin which gets expressed in mature adipocytes (fig 1F, panel ii). Interestingly, the promoter of
447 *Cebpd*, which regulates *Pparg* expression did not show any enhanced butyrylation in its promoter on day
448 3 and instead, exhibited increased butyrylation on day 6 of adipogenesis (fig 1F, panel iii). Collectively
449 these results showed that during adipogenesis, EP300 catalysed butyrylation of histones could be an
450 important epigenetic signature.

451

452 **Identification of a small molecule that selectively inhibits p300 catalysed histone butyrylation *in vitro*:**

453 In order to investigate the contribution of p300 catalyzed butyrylation per se in adipogenesis, we
454 adopted a chemical biology based approach. For this purpose, a series of derivatives of garcinol, a
455 polyisoprenylated benzophenone isolated from *Garcinia indica*, were synthesized (8). These derivatives,
456 unlike garcinol, were found to be non-toxic to cells and showed a high specificity towards the catalytic
457 activity inhibition of EP300. The derivatives were generated by internal cyclisation of garcinol with
458 further addition of one or two functional groups to the remaining free -OH groups- giving rise to mono

459 and disubstituted derivatives (Sup. fig. 1A). Amongst these, a few monosubstituted derivatives could
460 potently inhibit EP300 catalysed acetylation as well as butyrylation, while their disubstituted
461 counterparts were unable to inhibit acetylation (Sup. fig. 2 B, C and D). This was probably due to
462 increased steric hindrance brought about by the addition of an extra functional group that interfered
463 with the interaction between the compounds and EP300.

464 An inverse correlation between catalytic rates of acylation reactions by EP300 and increasing acyl chain
465 length had already been established previously (9). Based on this, we hypothesized since butyrylation is
466 catalysed by EP300 at a much slower rate than acetylation, one of the compounds that could not inhibit
467 EP300 catalysed acetylation might be able to inhibit the slower butyrylation reaction. Our *in vitro*
468 butyrylation assay using recombinant p300 and histone H3 as the substrate revealed a few potential
469 candidates (Sup. Fig. 2 E) as butyrylation inhibitors. Amongst them, LTK-14A, which is 13, 14 dimethoxy
470 isogarcinol, was capable of inhibiting full length EP300 catalysed butyrylation at a concentration of 25
471 μM (fig. 2 C and D), with minimal effect on EP300 catalysed acetylation in similar reaction conditions (fig.
472 2 A and B).

473 In order to understand the underlying mechanism of the selective inhibition by LTK-14A, we performed
474 molecular docking analysis of LTK-14A (Fig. 2 G) and the catalytic domain. To delineate this, we solved
475 the crystal structure of LTK-14A (Table 1, Sup. Fig.2A). LTK-14 (fig. 2E), a specific inhibitor of EP300
476 catalysed acetylation and butyrylation (Sup. Fig. 2 B and C) was used for further comparative analysis.
477 The energy minimized analysis revealed that both LTK-14 and LTK-14A could potentially bind with the
478 active site of the EP300 catalytic domain forming several hydrophobic interactions (Fig.2 F and H). LTK-
479 14, due to the presence of a free phenolic –OH group, could hydrogen bond with a carbonyl oxygen
480 atom present in the peptide backbone of S1396 residue. However, LTK-14A has all of its phenolic –OH
481 groups blocked and so it is incapable of forming such an interaction. This hydrogen bonding by LTK-14

482 could imply a stronger binding to the enzyme, while LTK-14A, by interacting with fewer residues
483 presumably inhibits only the slower butyrylation reaction and the interaction may not be strong enough
484 to deter the faster acetylation reaction.

485 Some of the residues with which LTK-14A could potentially form hydrophobic interaction have already
486 been reported before as being critical for targeting inhibition of the enzymatic activity of EP300 by the
487 first reported EP300 inhibitor lysyl CoA (10). These residues include C1438, Y1446, Y1397 and W1436. To
488 verify this observation we generated a point mutant of p300 catalytic domain in which cysteine 1438,
489 showing the highest propensity to interact with LTK-14A, was mutated to alanine. We found that the
490 C1438A catalytic domain is equally active as the wild-type catalytic domain in an *in vitro* lysine
491 acetyltransferase assay (Sup. Fig. 2B). We observed that the wild-type EP300 catalytic domain catalysed
492 butyrylation was inhibited by LTK-14A most prominently at 25 µM concentration while acetylation was
493 not inhibited (compare lane 6 in each of fig.2 I-L). In contrast, neither acetylation nor butyrylation
494 modification catalysed by the mutant EP300 catalytic domain could be inhibited by LTK-14A even at 25
495 µM concentration (compare lane 6 in each of fig. 2 M-P). Altogether, these data suggest that LTK-14A
496 indeed interacts with C1438 within the active site of the EP300 catalytic domain, and this residue is
497 critical for its interaction to bring about butyrylation reaction inhibition.

498 **LTK-14A is a metabolically stable, cell permeable compound that significantly inhibits adipogenesis:**

499 Upon establishing that LTK-14A is an EP300 acylation-specific inhibitor *in vitro*, its cellular effects were
500 tested using 3T3L1 cells. The quality of our compound used in all biological experiments was acceptably
501 good with more than 97% purity (Sup. Fig. 2 C, D and E). We found the LTK14A is highly cell-permeable
502 and metabolically stable as it could be detected by mass spectrometry analysis from metabolites
503 extracted from LTK-14A treated cells after six days (Fig. 3A). MTT assay showed that LTK-14A at 25 µM
504 concentration did not have any adverse effect on the cellular oxidoreductase activity, a signature of

505 metabolic output of cells, (Fig. 3B) suggesting that LTK-14A is non-toxic to 3T3L1 even after 6 days of
506 treatment. Oil Red-O staining of 3T3L1 cells differentiated in the presence of LTK-14A followed by
507 spectrophotometric quantitaion revealed significant inhibition of adipogenesis by the compound (Fig.
508 3C, D).

509 In order to understand the transcriptional mechanism of LTK14A-mediated butyrylation inhibition on
510 adipogenesis, adipogenic cells were treated with LTK-14A and subjected to transcriptome analysis. We
511 used untreated and solvent treated cells as control. Volcano plot (Fig. 3E) and heat map analysis (Fig. 3F)
512 revealed that upon treatment with the compound, a large number of genes were differentially
513 expressed compared to DMSO treated and untreated conditions. To better understand the LTK-14A
514 affected genes, we focused on the common genes that were differentially expressed in the two cases-
515 (1) LTK-14A versus no inhibitor and (2) LTK-14A versus DMSO. Among these common genes, 2200 genes
516 were found to be downregulated and 1309 genes were upregulated (Fig. 4A) with a majority of them to
517 be protein coding genes (Fig. 4B). Gene ontology analysis revealed that LTK14A treatment
518 predominantly affected the genes involved in lipid metabolism pathways (Fig. 4C, E) which were
519 minimally affected by DMSO alone (Fig. 4D). The gene regulatory networks and the respective pathways
520 were constructed with the major genes that were affected by LTK-14A treatment compared to DMSO
521 treated and untreated conditions (Fig. 4F, Sup. Fig.3A). They collectively depict how LTK-14A, by
522 inhibiting expression of a large number of genes that are interconnected via several pathways
523 associated with lipid metabolism, brings about a collapse in the adipogenesis process as a whole.

524 A few of the pro-adipogenic genes downregulated by LTK-14A, as indicated by RNA sequencing, were
525 selected for further validation (Sup. Fig. 3B). RT-qPCR analysis corroborated that except for *Cebpd*, most
526 of the other pro-adipogenic genes (*Pparg, Cebpa, Adipoq, Lep, Slc2a4, Fasn* and *Fabp4*) showed a
527 marked downregulation upon LTK-14A treatment (Fig. 4G). *Acss2* was also downregulated by LTK-14A

528 (Sup. Fig.4C). The upregulation of anti-adipogenic genes was also verified by performing RT-qPCR
529 analysis for two such candidate genes- *Kdm4c* and *Tead4* (Sup. Fig.3C). Collectively, the RNA sequencing
530 analysis and the validation of gene targets further convincingly suggested that LTK-14A can inhibit
531 adipogenesis in 3T3L1 cells, mainly by repressing the expression of important pro-adipogenic genes.

532

533 **LTK-14A inhibits histone butyrylation in 3T3L1 cells, without affecting acetylation or other post-**
534 **translational modifications:**

535 Furthermore we wanted to find out whether LTK-14A mediated downregulation of adipogenesis is
536 causally linked to the inhibition of histone butyrylation in the 3T3L1 cells. We observed that treatment
537 with LTK-14A inhibited overall butyrylation of histones (Fig. 5 A, B). Among the specific modification sites
538 tested, H3K23 and H4K5 butyrylation showed a significant decrease upon treatment with LTK-14A (Fig. 5
539 A, B) while butyrylation at other tested sites were affected minimally (Sup. Fig. 3D). Acetylation of
540 histones (H3K9, H3K18 and H4K12) was also found to be unaffected (Fig. 5 C, D) upon LTK-14A
541 treatment. To establish the specificity of the LTK14A, the effect of LTK-14A on lysine and arginine
542 methylation along with phosphorylation of histones were also investigated. We observed (Fig. 5 E, F) no
543 significant changes in these marks upon the compound treatment, thereby indicating that in the 3T3L1
544 cells, LTK-14A specifically inhibits butyrylation.

545

546 **Inhibition of butyrylation attenuates weight gain of high fat diet fed C57BL6/J mice:**

547 After observing the anti-adipogenic effect of LTK-14A on 3T3L1 cells, we investigated whether this
548 compound could also affect adipogenesis and obesity at an organismal level. For this purpose, C57BL6/J
549 mice were maintained either on a normal diet or a high fat diet with or without LTK-14A. In due course

550 of time it was observed that the mice maintained on a high fat diet along with LTK-14A had a weight
551 gaining trend intermediate between the normal diet and high fat diet fed mice (Fig.6A,B). Dissection of
552 the mice revealed that the fat accumulation in high fat diet maintained mice was the highest, followed
553 by those on high fat diet and LTK-14A, and then by those on normal diet (Fig. 6C). The epididymal fat
554 pads were separately weighed and again it was observed that weights of the fat pads from compound
555 treated mice were much less than that of high fat diet fed mice (Fig. 6 D,E). The diet consumption
556 pattern of the mice showed that the two groups on high fat diet with or without LTK-14A, had a similar
557 consumption rate indicating that the reduced weight gain of the compound treated mice is not due to
558 discrepancy in diet consumption (Table 2). Hematoxylin and eosin staining of adipose tissue and liver
559 (Fig. 6 F,G) showed signs of adipocyte hypertrophy and hepatic steatosis in high fat diet fed mice, which
560 were absent in the mice maintained on normal diet or high fat diet with LTK-14A.

561 Immunofluorescence staining of the liver tissue samples revealed that there was a significant increase in
562 H4K5 butyrylation levels in high fat diet fed mice compared to normal diet fed mice in which the
563 modification was barely detectable and it was almost completely inhibited upon LTK-14A treatment (Fig.
564 6H panel iii, Fig. 6I panel iii). On the other hand, no significant difference in H4K12 (Fig. 6H panel i, Fig. 6I
565 panel i) and H3K14 acetylation (Fig. 6H panel ii, Fig. 6I panel ii) levels could be observed across all the
566 three groups. Furthermore, histone modification pattern in the adipose tissues was studied with acid
567 extracted histones from the epididymal fat pads. H4K5 butyrylation was reduced in the LTK-14A treated
568 samples compared to those of high fat diet fed mice (Fig. 6 J, N) while H3K14, H3K18 and H4K12
569 acetylation levels were relatively unchanged across all the three groups (Fig. 6 J, K, L, M). The metabolic
570 stability of LTK-14A in mice was verified by its detection in ESI spectra of analytes extracted from the
571 liver of compound treated mice (Sup. Fig 3 E).

572 **The butyrylation specific inhibitor reduces weight of genetically obese db/db mice:**

573 The previous model system involved the use of LTK-14A as a prophylactic. To test whether LTK-14A
574 could also reduce obesity by inhibiting histone butyrylation, genetically obese homozygous mutant
575 db/db mice were used. Heterozygous mutant db+/- mice were taken as control. The hyperphagic db/db
576 mice were orally administered LTK-14A daily at the same dosage as before (50 mg/Kg body weight). We
577 observed that upon oral gavaging of LTK-14A, the overweight mice not only showed an arrest in weight
578 gain, but their body weights were significantly reduced by the end of one month of treatment (Fig. 7
579 A,B,C). The food intake of LTK-14A treated mice was marginally less than that of the vehicle treated mice
580 (Table 2, Supplementary Information), although both groups consumed more food compared to the
581 db+/- mice during the treatment regime. Average weight of the liver (Fig. 7 D,E) and epididymal fat pads
582 (Fig. 7 F,G) was the highest for db/db mice given vehicle control and least for the db+/- mice, while that
583 for the compound treated db/db mice was intermediate. *In vivo* Echo MRI of live mice revealed that
584 total adiposity i.e. fat mass of the mice was significantly lowered upon LTK-14A treatment (Fig. 7 H) and
585 lean mass was marginally affected (Fig. 7 I). Hematoxylin and eosin staining of adipose tissue and liver
586 (Fig. 7 J,K) showed signs of adipocyte hypertrophy and hepatocyte ballooning in vehicle treated db/db
587 mice, which were absent in the db+/- and LTK-14A treated db/db mice.

588 Similar to the high fat diet induced obesity model, the more obese homozygous leptin receptor mutant
589 mice (db/db) liver had greater level of H4K5 butyrylation compared to leaner heterozygous mutant mice
590 (db +/-) (Fig 7L panel iii, Fig. 7M panel iii). Moreover, LTK-14A treated db/db mice liver showed a
591 decrease in H4K5 butyrylation compared to vehicle control treated mice liver. In contrast, H4K12 (Fig. 7L
592 panel i, Fig. 7M panel i) and H3K14 acetylation (Fig. 7L panel ii, Fig. 7M panel ii) were only partially
593 upregulated in the db/db mice and did not get significantly reduced upon LTK-14A treatment.
594 Immunoblotting with acid extracted histones from epididymal fat pads showed that H4K5 butyrylation
595 was reduced in the adipose tissues of LTK-14A treated mice (Fig. 7 N,R) compared to vehicle control
596 treated obese mice. H3K14, H3K18 and H4K12 acetylation were not significantly altered in any of the

597 three groups (Fig. 7 N,O,P,Q). Finally, RT-qPCR analysis showed that just like in cellular model of
598 adipogenesis, LTK-14A treatment led to robust inhibition of important pro-adipogenic genes *Pparg*, *Lep*,
599 *Slc2a4* and *Adipoq* in the fat pads of compound treated db/db mice (Fig. 7S). Collectively these data
600 establish that obesity can not only be prevented but also reverted by specific inhibition of H4K5
601 butyrylation, thereby highlighting the importance of this modification in the context of adipogenesis.

602 **LTK-14A is non-mutagenic and non-toxic in nature for biological applications:** Based on the
603 observations of obesity attenuating effects of LTK-14A in two different mice models, we performed
604 some preclinical tests to ensure that the obesity arrest was not as a result of any deleterious side effect
605 of toxicity from the compound. Plate incorporation assay was carried out in four different nutritional
606 auxotrophic mutants of Salmonella typhimurium (TA97a, TA98, TA100 & TA102)in absence or presence
607 of rat liver extract (S9 enzyme fraction). It was observed that the number of revertants obtained from
608 LTK-14A was similar to that from vehicle control and far less compared to that from the positive control
609 in all four strains, both in the absence and presence of liver extract (Sup. Fig 4 A-H). Furthermore, acute
610 toxicity test was performed in rats for checking whether a single administration of excessively high dose
611 of LTK-14A would alter the body weight and food/water consumption pattern of the rats. The body
612 weight changes in the LTK-14A administered rats were similar to the vehicle control treated ones (Table
613 6) with no gross morphological changes in any organ. Moreover, there was also no significant treatment
614 related effect on the food and water consumption of rats of both gender for all three doses compared to
615 vehicle control (Table 6).

616 Collectively these data imply that LTK-14A does not have deleterious toxic effects on the test animals
617 and could have a potential for downstream applications for tackling obesity related complications.

618

619

620

621 **Discussion**

622 Reports on the physiological relevance of acylation modifications are scanty. Breakthroughs have been
623 made in establishing the importance of butyrylation in spermatogenesis (5), β-hydroxybutyrylation in
624 starvation response (11) and crotonylation in inflammatory response, digestive system, cancer and HIV
625 latency (7,12,13,14). Lysine propionylation has also been reported as an activation mark on histones
626 that could be useful in various physiological processes (15). The list of these modifications seems to be
627 increasing continuously, with the recent additions of histone serotonylation (16), lactylation (17) and
628 dopaminylation (18). The fact that serotonin and dopamine are chemical neurotransmitters while
629 lactate is derived from pyrvate, a glycolytic end product, and all these molecules bring about
630 modification of histones thereby mediating gene expression in several tissues, bear testimony to the
631 hypothesis that the abundance levels of cellular metabolites in different physiological contexts can lead
632 to modification of histones with a plethora of diverse chemical moieties that can selectively modulate
633 gene expression patterns.

634 Our initial experiments in 3T3L1 adipogenesis indicated an important role of ACSS2 in the differentiation
635 process by generating butyryl CoA for histone butyrylation. Inside the cells ACL (ATP citrate lyase) and
636 ACSS2 that have been implicated in generation of nuclear acetyl CoA. Both the enzymes are known for
637 regulating gene expression in different contexts by acetylating histones in specific genomic loci (19-21).
638 Knockdown of *Acss2* had a much more pronounced effect on H4K5 butyrylation compared to H3K18
639 acetylation. This is probably due to the fact that ACSS2 is the sole/major producer of acyl CoA species
640 while acetyl CoA can be generated by diverse means and knockdown of a single acetyl CoA producer
641 was not enough to have a robust effect on global acetylation level of histones. Similar observations have
642 already been made for histone crotonylation in HeLa cells (7).

643 Due to redundancy in the functionality of p300 catalyzed butyrylation with acetylation, the significance
644 of butyrylation in adipogenesis was demonstrated using a pharmacological approach. LTK-14A could
645 selectively and specifically inhibit histone butyrylation and still inhibit adipogenesis by downregulating
646 expression of many pro-adipogenic genes. However amongst these genes *CEBPd* expression did not get
647 affected by LTK-14A possibly because the expression of this gene is less prone to be regulated by histone
648 butyrylation in its promoter. Indeed, chromatin immunoprecipitation study indicated that in the initial
649 stage of induction of differentiation in pre-adipocytes, there was no enrichment of H4K5 butyrylation in
650 the promoter of *Cebpd*. This could explain why the butyrylation inhibitor LTK-14A treatment at the
651 induction stage did not inhibit *Cebpd* expression, since there was no buyrylation mark enrichment for
652 inhibition in its promoter to begin with. An increased butyrylation in its promoter at the terminal stage
653 could be either through p300 catalysed modification or non-enzymatic means with greater availability of
654 butyryl CoA, or both. Currently, we have not been able to verify this. However our preliminary
655 observations with promoter specific studies indicate that H4K5 butyrylation plays a role in regulating the
656 expression of the critical transcription factor *Pparg*. Inhibition of butyrylation by LTK-14A repressed the
657 expression of the master regulator which further led to the inhibition of downstream genes like *Lep*,
658 whose expression is dependent on PPARγ. While cell line based studies indicate that C/EBPδ regulates
659 the expression of a cascade of transcription factors like C/EBPα and PPARγ, this fact has been
660 questioned in knockout mice which have poorly differentiated adipose tissue but still express *Pparg* and
661 *Cebpa* (22). This indicates that there could be other factors playing a redundant function like C/EBPδ in
662 the initiation stage of adipogenesis. Moreover, an additional function of C/EBPδ may seem to be
663 downstream of C/EBPα and PPARγ at the terminal stage of adipogenesis. It has been speculated that this
664 could involve inducing the expression of ligands that activate PPARγ (23). Therefore, the increased
665 butyrylation in the promoter of *Cebpd* on day 6 of adipogenesis might be responsible for its role in the

666 terminal stage. The expression of *Cebpd* is independent of *Pparg* and hence repression of *Pparg* by
667 butyrylation inhibition with LTK-14A did not repress *Cebpd*.

668 *Acss2*, which encodes the enzyme responsible for butyryl CoA biosynthesis was also downregulated by
669 LTK-14A which might have further contributed to reduced butyrylation of histones during inhibition of
670 adipogenesis. Amongst the different histone modification patterns investigated, H4K5 butyrylation was
671 consistently affected by LTK-14A in different cell line and mice models, while the other site specific
672 butyrylation marks were relatively unaltered, indicating that there may be a hierarchy in the importance
673 of these modifications in regulation of adipogenesis. While our work was in progress, a new report was
674 published in which it was demonstrated that inhibition of fatty acid synthesis as well as oxidation leads
675 to reduction in H4K5 butyrylation while acetylation remains unaffected (24). This further reinforces our
676 own hypothesis that fatty acid metabolism is an important source for certain acyl CoAs such as butyryl
677 CoA, derived from the short chain fatty acid butyric acid. Another work published during this period
678 revealed HBO1, a member of MYST family of acetyltransferase, also possesses the ability to catalyse
679 acylation reactions including butyrylation (25). Mass spectrometry studies of histone modifications
680 altered by knockdown of HBO1 in HeLa cells showed that H4K5 butyrylation does not get affected by
681 depletion of HBO1 indicating that it is a p300 specific mark.

682 Global histone acetylation has previously been reported to remain unchanged in liver and adipose
683 tissues of mice even after high fat diet consumption (26), which was consistent with the observations we
684 made in both mice models studied. Since acetyl CoA is highly abundant, fluctuations in its levels did not
685 lead to major changes in histone acetylation pattern. Because the usual butyryl CoA levels are far less
686 than their corresponding Michaelis Menten constant for p300, an increase in butyryl CoA levels due to
687 excess lipid consumption through high fat diet or *de novo* lipid synthesis through excess food
688 consumption, resulted in a concomitant increase in butyrylation by p300 which served as the nutritional

689 sensor for butyryl CoA. Enhanced H4K5 butyrylation was not observed in mature adipose tissues of
690 obese mice possibly due to predominance of adipocyte population in the tissues of mice from all the
691 groups (27).

692 In the 21st century, obesity has become a major epidemic leading to several other disorders such as
693 type 2 diabetes and arteriosclerosis. Histone acetylation inhibition could be regarded as a possible
694 method for attenuating adipogenesis and obesity. But acetylation is a widespread phenomenon that is
695 required in several other physiological processes besides adipogenesis. Hence, treatment with an
696 acetyltransferase inhibitor at a particular range of concentration could have undesirable side effects and
697 toxicity. In contrast, butyrylation is a rarer event, repressing which may be less harmful to other
698 processes. Indeed, our preclinical tests are indicative of the fact that LTK-14A may be suitable for
699 development as a possible anti-obesity drug due to its negligible toxicity side effects. The present finding
700 thus establishes an importance of histone butyrylation in adipogenesis, making it an attractive target for
701 pharmacological inhibition of adipogenesis and thereby controlling obesity (Graphical abstract).

702 **References**

703 **1.** Haws, S. A., Leech, C. M., Denu, J. M. Metabolism and the Epigenome: A Dynamic Relationship.
704 Trends Biochem 2020; 45, 731-747

705 **2.** Chen, Y., Sprung, R., Tang, Y., Ball, H., Sangras, B., Kim et al Lysine propionylation and
706 butyrylation are novel post-translational modifications in histones. Mol Cell Proteomics 2007; **6**:
707 812-819

708 **3.** Goudarzi, A., Zhang, D., Huang, H., Barral, S., Kwon, O. K., Qi, S. et al Dynamic Competing
709 Histone H4 K5K8 Acetylation and Butyrylation Are Hallmarks of Highly Active Gene Promoters.
710 Mol Cell 2016;**62**:169-180

711 **4.** Yoo, E. J., Chung, J. J., Choe, S. S., Kim, K. H., and Kim, J. B. Down-regulation of histone
712 deacetylases stimulates adipocyte differentiation. J Biol Chem 2006; **281**:6608-6615
713 **5.** Wellen, K. E., Hatzivassiliou, G., Sachdeva, U. M., Bui, T. V., Cross, J. R., and Thompson, C. B. ATP-
714 citrate lyase links cellular metabolism to histone acetylation. Science 2009;**324**:1076-1080
715 **6.** King, M. T., and Reiss, P. D. Separation and measurement of short-chain coenzyme-A
716 compounds in rat liver by reversed-phase high-performance liquid chromatography. Anal
717 Biochem 1985;**146**:173-179
718 **7.** Sabari, B. R., Tang, Z., Huang, H., Yong-Gonzalez, V., Molina, H., Kong, H. E. et al Intracellular
719 crotonyl-CoA stimulates transcription through p300-catalyzed histone crotonylation. Mol Cell
720 2015;**58**:203-215
721 **8.** Mantelingu, K., Reddy, B. A., Swaminathan, V., Kishore, A. H., Siddappa, N. B., Kumar, G. V. et al
722 Specific inhibition of p300-HAT alters global gene expression and represses HIV replication.
723 Chem Biol 2007;**14**:645-657
724 **9.** Kaczmarska, Z., Ortega, E., Goudarzi, A., Huang, H., Kim, S., Márquez et al Structure of p300 in
725 complex with acyl-CoA variants. Nat Chem Biol 2017; **13**:21-29
726 **10.** Liu, X., Wang, L., Zhao, K., Thompson, P. R., Hwang, Y., Marmorstein, R. et al The structural basis
727 of protein acetylation by the p300/CBP transcriptional coactivator. Nature 2008;**451**:846-850
728 **11.** Xie, Z., Zhang, D., Chung, D., Tang, Z., Huang, H., Dai, L. et al Metabolic Regulation of Gene
729 Expression by Histone Lysine β-Hydroxybutyrylation. Mol Cell 2016;**62**:194-206
730 **12.** Fellows, R., Denizot, J., Stellato, C., Cuomo, A., Jain, P., Stoyanova, E. et al Microbiota derived
731 short chain fatty acids promote histone crotonylation in the colon through histone deacetylases.
732 Nat Commun 2018;**9**:105
733 **13.** Wan, J., Liu, H., and Ming, L. Lysine crotonylation is involved in hepatocellular carcinoma
734 progression. Biomed Pharmacother 2019;**111**:976-982

735 **14.** Jiang, G., Nguyen, D., Archin, N. M., Yukl, S. A., Méndez-Lagares, G., Tang, Y. et al HIV latency is
736 reversed by ACSS2-driven histone crotonylation. J Clin Invest 2018;**128**:1190-1198
737 **15.** Kebede, A. F., Nieborak, A., Shahidian, L. Z., Le Gras, S., Richter, F., Gómez, D. A. et al Histone
738 propionylation is a mark of active chromatin. Nat Struct Mol Biol 2017;**24**:1048-1056
739 **16.** Farrelly, L. A., Thompson, R. E., Zhao, S., Lepack, A. E., Lyu, Y., Bhanu, N. V. et al Histone
740 serotonylation is a permissive modification that enhances TFIID binding to H3K4me3. Nature
741 2019;**567**:535-539
742 **17.** Zhang, D., Tang, Z., Huang, H., Zhou, G., Cui, C., Weng, Y. et al. Metabolic regulation of gene
743 expression by histone lactylation. Nature **574**,575-580 (2019)
744 **18.** Lepack, A.E., Werner, C.T., Stewart, A.F., Fulton, S.L., Zhong, P., Farrelly, L.A. et al.
745 Dopaminylation of histone H3 in ventral tegmental area regulates cocaine seeking. Science **368**,
746 197-201 (2020)
747 **19.** Mews, P., Donahue, G., Drake, A.M., Luczak, V., Abel, T., Berger, S.L. Acetyl-CoA synthetase
748 regulates histone acetylation and hippocampal memory. Nature 2017; 546, 381–386
749 **20.** Wellen, K.E., Hatzivassiliou, G., Sachdeva, U.M., Bui, T.V., Cross, J.R., Thompson, C.B. ATP-
750 citrate lyase links cellular metabolism to histone acetylation. Science2009; 324, 1076–1080
751 **21.** Mews, P., Egervari, G., Nativio, R., Sidoli, S., Donahue, G., Lombroso, S.I. Alcohol metabolism
752 contributes to brain histone acetylation. Nature 2019; 574, 717–721
753 **22.** Tanaka, T., Yoshida, N., Kishimoto, T., Akira, S. Defective adipocyte differentiation in mice
754 lacking the C/EBPbeta and/or C/EBPdelta gene. EMBO J. 1997; 16, 7432–7443.
755 **23.** Hamm, J.K., Park, B.H., Farmer, S.R. A role for C/EBPbeta in regulating peroxisome proliferator-
756 activated receptor gamma activity during adipogenesis in 3T3-L1 preadipocytes. J. Biol. Chem.
757 2001; 276, 18464–18471.

758 **24.** Gao, M. et al. Metabolically controlled histone H4K5 acylation/acetylation ratio drives BRD4
759 genomic distribution. Cell Rep 2021; 36(4):109460.
760 **25.** Xiao, Y. et al. HBO1 is a versatile histone acyltransferase critical for promoter histone acylations.
761 Nucleic Acids Res 2021; 49(14):8037-8059.

762 **26.** Carrer, A., Parris, J. L., Trefely, S., Henry, R. A., Montgomery, D. C., Torres, A. et al Impact of a
763 High-fat Diet on Tissue Acyl-CoA and Histone Acetylation Levels. J Biol Chem 2017;**292**:3312-
764 3322
765 **27.** Burgeois, C., Gorwood, J., Barrail-Tran, A., Lagathu, C., Capeau, J., Desjardins, D. et al. Specific
766 Biological Features of Adipose Tissue, and their impact on HIV persistence. Front Microbiol **17**
767 (2019)

768 **28.** Trapnell, C., Roberts, A., Goff, L., Pertea, G., Kim, D., Kelley et al Differential gene and transcript
769 expression analysis of RNA-seq experiments with TopHat and Cufflinks. Nat Protoc 2012;**7**:562-
770 578

771 **29.** Thomas, P. D., Campbell, M. J., Kejariwal, A., Mi, H., Karlak, B., Daverman, R. et al PANTHER: a
772 library of protein families and subfamilies indexed by function. Genome Res 2003;**13**:2129-2141

773 **30.** de Hoon, M. J. L., Imoto, S., Nolan, J.,Miyano, S. Open source clustering software. Bioinformatics
774 2004;**9**:1453-1454

775

776

777 ## Figure legends:

778 **Fig.1 Histone butyrylation increases during adipogenesis** (A) Phase contrast images of 3T3L1 cells
779 exhibiting fibroblast like morphology in their pre-adipocyte state and accumulation of lipid droplets

780 in their adipocyte state. The lipid droplets can be stained using Oil Red-O dye. (B) RT-qPCR analysis
781 was performed to check for transcript levels of Acss2 in undifferentiated and differentiated 3T3L1
782 cells. Error bars denote mean +/- SEM of three biological replicates; two-tailed unpaired Student's t-
783 test: * P < 0.05, **P < 0.01, ***P < 0.001, ns: not significant. (C) Knockdown of Acss2 in
784 differentiated 3T3L1 cells was confirmed by RT-qPCR analysis. Error bars denote mean +/- SEM of
785 three biological replicates; two-tailed unpaired Student's t-test: * P < 0.05, **P < 0.01, ***P < 0.001,
786 ns: not significant. (D) Histone acetylation and butyrylation pattern in 3T3L1 cells upon Acss2
787 knockdown was checked using antibodies against acetylated histone H3K18 and butyrylated H4K5.
788 (E) Histone acetylation and butyrylation levels in 3T3L1 cells in undifferentiated and differentiated
789 state were analysed by immunoblotting with antibodies specific for acetylated H3K9, butyrylated
790 H3K9, H3K23, H3K27, H4K5, H4K8, H4K12 and pan-butyryl lysine antibodies . Antibodies against core
791 histones H3 and H4 were used as loading controls along with Direct Blue staining of all four core
792 histones. Lane 1- undifferentiated pre-adipocyte (Day 0) and Lane 2 - differentiated adipocyte (Day
793 7) in each of the panels i, ii and iii. (F) Enrichment of H4K5 butyrylation in the promoters of (i) Pparg,
794 (ii) Lep and (iii) Cebpd represented in the form of fold change over IgG. Error bars denote mean +/-
795 SEM of three biological replicates; one-way ANOVA with Dunnett's multiple comparision was
796 performed: * P < 0.05, **P < 0.01, ***P < 0.001, ns: not significant.

797 **Figure 2: LTK-14A selectively inhibits p300 catalysed butyrylation without affecting its**
798 **acetyltransferase activity:** Immunoblotting with antibodies against acetylated H3K18 (A) and pan-
799 butyryl lysine (C) to check for the relative inhibition of acetyltransferase and butyryltransferase
800 activities of full length p300 by LTK-14A at different concentrations. Recombinant histone H3 was
801 used as substrate. Lane 1, enzyme alone; Lane 2, enzyme + DMSO; Lane 3-6, enzyme + LTK-14A at
802 concentrations 10, 15, 20 and 25 µM respectively. Images of Western blotting are given in panels F
803 and H and their quantitations are given in panels B and D. Molecular structures of mono- (LTK-14)

804 and di-(LTK-14A) substituted isogarcinol (E and G). Molecular docking studies for studying
805 comparative interaction of LTK-14 and LTK-14A with the amino acid residues of p300 catalytic
806 domain (F and H). The predicted interactions are denoted by tick lines. Hydrogen bonding is shown
807 in red and hydrophobic interaction is shown in green. Immunoblotting with antibodies against
808 acetylated H3K18 (I) and pan-butyryl lysine (K) to check for the relative inhibition of
809 acetyltransferase and butyryltransferase activities of wild type p300 catalytic domain by LTK-14A at
810 different concentrations. Lane 1, enzyme alone; Lane 2, enzyme + DMSO; Lane 3-6, enzyme + LTK-
811 14A at concentrations 10, 15, 20 and 25 µM respectively. Images of Western blotting are given in
812 panels I and K and their quantitations are given in panels J and L. Immunoblotting with antibodies
813 against acetylated H3K18 (M) and pan-butyryl lysine (O) to check for the relative inhibition of
814 acetyltransferase and butyryltransferase activities of catalytically active p300 catalytic domain with
815 point mutation C1438A by LTK-14A at different concentrations. Lane 1, enzyme alone; Lane 2,
816 enzyme + DMSO; Lane 3-6, enzyme + LTK-14A at concentrations 10, 15, 20 and 25 µM respectively.
817 Images of Western blotting are given in panels M and O and their quantitation are given in panels N
818 and P. Error bars denote mean +/- SEM of three biological replicates, one-way ANOVA with
819 Bonferroni's multiple comparison; * $P < 0.05$, ** $P < 0.01$, *** $P < 0.001$, ns: not significant.

820 **Fig. 3: The butyrylation inhibitor represses adipogenesis in 3T3L1 cells:** (A) The permeability and
821 stability of LTK-14A in 3T3L1 was tested by LC-ESI-MS analysis of metabolites, extracted from the
822 compound treated 3T3L1 cells to detect the protonated LTK-14A in the ESI spectra of the eluted
823 fraction. (B) MTT assay was performed to check for any possible cellular toxicity effect of LTK-14A,
824 using 25 µM concentration of the compound on 3T3L1 cells upon incubation for varying lengths of
825 time (2, 4 and 6 days). Comparison was done with cells that were left untreated or treated with
826 DMSO as solvent control. The effect of LTK-14A (25 µM) treatment on adipogenesis was tested by
827 Oil Red-O staining of the adipocytes (C) and the quantitation of staining is represented graphically in

828 panel D. Error bars denote mean +/- SEM of three biological replicates,one-way ANOVA with
829 Bonferroni's multiple comparison; * P < 0.05, **P < 0.01, ***P < 0.001, ns: not significant. (E) The
830 effect of LTK-14A on the global transcription network inside 3T3L1 cells was investigated by high
831 throughput transcriptome analysis with RNA isolated from compound treated, DMSO treated and
832 untreated 3T3L1 cells (n=2 in each case). Differential gene expression pattern of three conditions
833 compared with each other, depicted in volcano plots- No Inhibitor versus DMSO , No Inhibitor
834 versus LTK-14A and DMSO versus LTK-14A. The downregulated and upregulated genes are shown in
835 blue and red respectively.(F) Heat maps showing the differential gene expression pattern between
836 LTK-14A treated cells and DMSO treated or untreated cells.

837 **Figure 4: LTK-14A represses expression of several pro-adipogenic genes and inhibits lipid**
838 **metabolism:** (A) Venn diagram showing the number of differentially expressed genes upon LTK-14A
839 treatment with respect to untreated and DMSO treated conditions. (B) Classification of the common
840 differentially expressed genes according to their type. Gene ontology analysis was performed to
841 study the different biological pathways that were affected by LTK-14A in 3T3L1 compared to DMSO
842 treated as well as untreated conditions, as predicted by Panther software. The pathways were
843 ranked in the order of those with maximum number of genes affected (E). A different ranking order
844 was created on the basis of fold enrichment i.e. the pathways in which the ratio of number of
845 observed affected genes over number of expected genes to be affected was the highest (C). A
846 similar analysis was also performed for genes differentially expressed in DMSO versus untreated
847 conditions (D). (F) A molecular network was constructed to depict the interconnectivity between the
848 lipid metabolism related genes and pathways that were affected upon their dysregulation by LTK-
849 14A compared to DMSO treated conditions. (G) RT-qPCR analysis was performed to validate the
850 putative target genes of LTK-14A. Error bars denote mean +/- SEM of three biological replicates;

851 one-way ANOVA with Bonferroni's multiple comparison: * P < 0.05, **P < 0.01, ***P < 0.001, ns:
852 not significant.

853

854 **Fig.5: LTK-14A inhibits histone butyrylation in 3T3L1 cells, without affecting acetylation or other**
855 **post-translational modifications**: Histone butyrylation levels in 3T3L1 cells that were treated with
856 LTK-14A were compared with that in DMSO treated and untreated conditions by immunoblotting
857 with antibodies against butyrylated histone H3K23 , H4K5 and pan-butyryl lysine. Histones H3 and
858 H4 were used as loading controls (A). The fold change of quantified band intensity is graphically
859 represented in panel (B) in which the error bars denote mean +/- SEM of three biological replicates.
860 Under similar conditions histone acetylation levels were compared by immunoblotting using
861 antibodies against acetylated histones H3K18, H3K9 and H4K12 (C). The result is graphically
862 represented in panel (D) in which error bars denote mean +/- SEM of three biological replicates.
863 Immunoblotting was also performed with antibodies against histone H3R17 dimethylation, H3S10
864 Phosphorylation and H3K9 dimethylation (E). The result is graphically represented in panel F in
865 which error bars denote mean +/- SEM of three biological replicates. For all data one-way ANOVA
866 with Bonferroni's multiple comparision was performed: * P < 0.05, **P < 0.01, ***P < 0.001, ns: not
867 significant .

868 **Fig. 6: The weight gaining of high fat diet fed mice (C57BL6/J) could be significantly reduced by the**
869 **butyrylation specific inhibitor of p300:** Trend of weight gaining (A) and average body weight gained
870 after 16 weeks (B) of C57BL6/J mice maintained on normal chow diet, high fat diet and high fat diet
871 mixed with LTK-14A was plotted; n=4 in each group. Representative images of dissected bodies
872 showing fat accumulation (C) and epididymal fat pads (D) of the mice from three groups. The
873 average weight of the fat pads is represented graphically (E); n=4 in each group. Representative

874 images of morphology of adipose tissue (F) and liver (G) from the mice of the three groups, as
875 studied by hematoxylin and eosin staining. For all data one-way ANOVA with Dunnett's multiple
876 comparision was performed: * P < 0.05, **P < 0.01, ***P < 0.001, ns: not significant. (H)
877 Immunofluorescence microscopy of liver sections stained with antibodies against histone H4K12
878 acetylation (panel i), histone H3K14 acetylation (panel ii) and histone H4K5 butyrylation (panel iii).
879 The fluorescence intensity of the modified histone marks was normalised against DAPI staining of
880 whole nuclei for quantitation which is graphically depicted in (I) panel i, ii and iii ;n=4 in each group;
881 one-way ANOVA with Dunnett's multiple comparision: * P < 0.05, **P < 0.01, ***P < 0.001, ns: not
882 significant. (J) Histone H3K14, H3K18, H4K12 acetylation and H4K5 butyrylation levels in epididymal
883 fat pads of mice were estimated by immunoblotting . Histone H3 was used as loading control The
884 fold change of quantified band intensity is graphically represented in panel K,L, M and N ;n=3 in each
885 group; one-way ANOVA with Dunnett's multiple comparision: * P < 0.05, **P < 0.01, ***P < 0.001,
886 ns: not significant.

887 **Fig. 7: Oral gavaging of the butyrylation inhibitor reduces weight of genetically obese db/db mice:**
888 Trend of weight gaining (A) and average body weight gained after 30 days (B) of db +/- and db/db
889 mice orally administered with either LTK-14A or vehicle solution ; n=6 in each group. (C)
890 Representative images of dissected bodies showing fat accumulation (panel iii) of the mice from
891 three groups. Representative images of liver (D) from the mice of three groups and average weight
892 of liver (E) depicted graphically; n= 6 in each group. Representative images of epididymal fat pads (F)
893 from the mice of three groups and average weight of fat pads (G) depicted graphically; n= 6 in each
894 group. Total fat mass (H) and total lean mass (I) of mice from three groups are depicted graphically;
895 n= 6 in each group. Representative images of morphology of liver (J) and adipose tissue (K) from the
896 mice of the three groups, as studied by hematoxylin and eosin staining. (L) Immunofluorescence
897 microscopy of liver sections stained with antibodies against histone H4K12 acetylation (panel i),

898 histone H3K14 acetylation (panel ii) and histone H4K5 butyrylation (panel iii). The fluorescence
899 intensity of the modified histone marks was normalised against DAPI staining of whole nuclei for
900 quantitation which is graphically depicted in (M) panel i, ii and iii ;n=4 in each group; one-way
901 ANOVA with Dunnett's multiple comparision: * P < 0.05, **P < 0.01, ***P < 0.001, ns: not
902 significant. (N) Histone H3K14, H3K18, H4K12 acetylation and H4K5 butyrylation levels in epididymal
903 fat pads of mice were estimated by immunoblotting. Histone H3 was used as loading control The
904 fold change of quantified band intensity is graphically represented in panel O,P, Q and R; n=3 in
905 each group; one-way ANOVA with Dunnett's multiple comparision: * P < 0.05, **P < 0.01, ***P <
906 0.001, ns: not significant. (S) qRT-PCR with RNA isolated from epididymal fat pads to check the
907 expression pattern of lipogenesis related pro-adipogenic genes upon LTK-14A treatment;
908 n=3/4 in each group; one-way ANOVA with Dunnett's multiple comparision: * P < 0.05, **P
909 < 0.01, ***P < 0.001, ns: not significant

910 **Graphical abstract:**

911 **Proposed model for the role of p300-mediated histone butyrylation in adipogenesis:**

912 In pre-adipocytes, there exists a basal level of histone acetylation while butyrylation is present to a
913 much lesser extent owing to low stoichiometric levels of butyryl CoA. Induction of adipogenesis
914 causes a simultaneous upregulation of histone acetylation and butyrylation marks leading to
915 increased rate of adipogenesis and concomitant transcriptional activation of pro-adipogeneic genes.

916 Onset of obesity in mice, either due to excess energy intake through high fat diet consumption or
917 increased de novo synthesis of fatty acids due to leptin receptor gene mutation leading to
918 hyperphagic behavior, is accompanied by adipocyte hyperplasia and hypertrophy. Both the organs
919 of adipose tissue and liver were found to have enhanced levels of H4K5 butyrylation during obesity.

920 LTK-14A, a butyrylation specific inhibitor could efficiently prevent the processes of adipogenesis and
921 adipocyte hypertrophy due to inhibition of H4K5 butyrylation in these organs. Thus the compound
922 could attenuate weight gain by selective inhibition of butyrylation without affecting acetylation,
923 thereby highlighting the importance of histone butyrylation in adipogenesis and obesity.

924

925

926

927

928

929

Figure 1

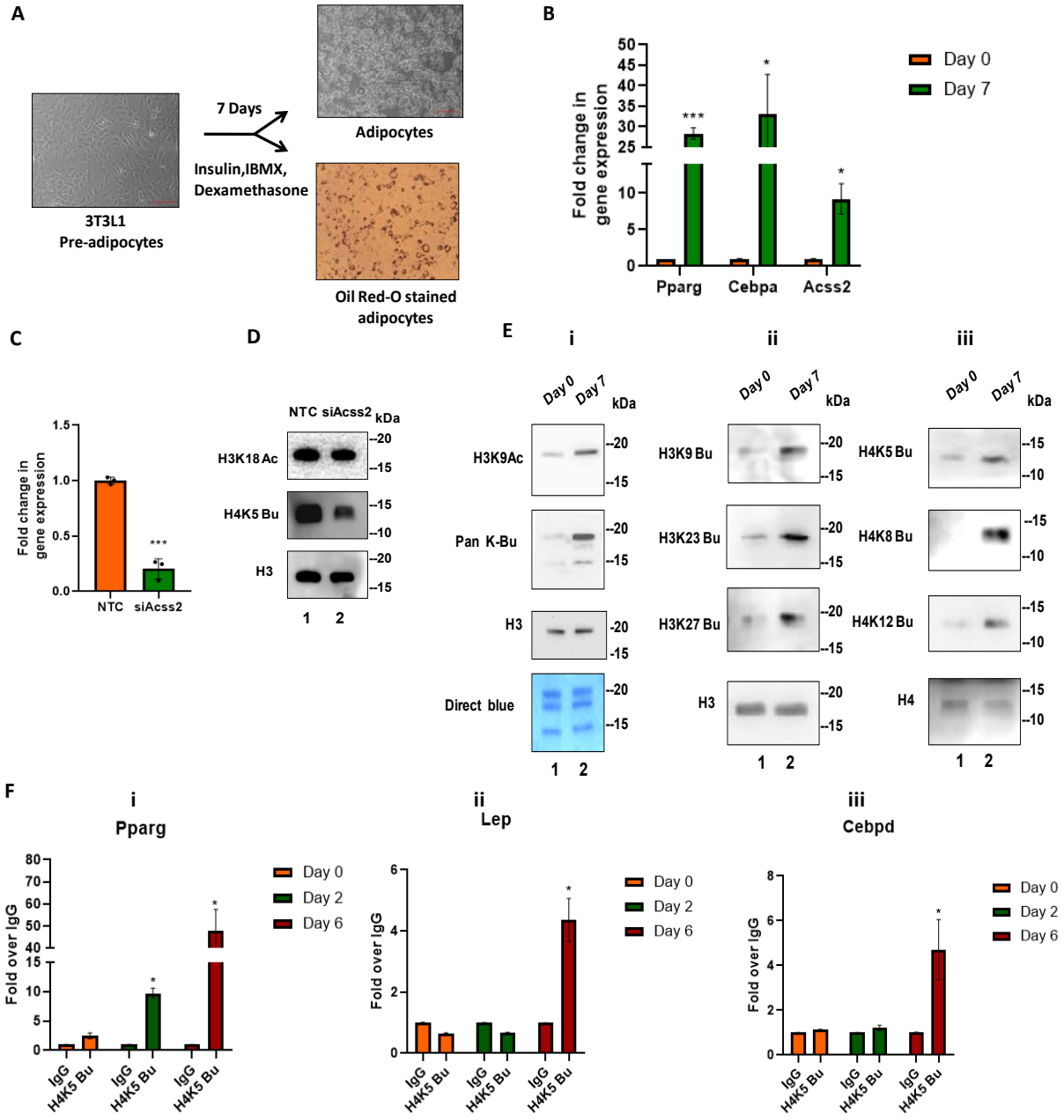
A
3T3L1
Pre-adipocytes
7 Days
Insulin,IBMX,
Dexamethasone
Adipocytes
Oil Red-O stained
adipocytes
B
Fold change in
gene expression
Day 0
Day 7
Pparg
Cebpa
Acss2
C
Fold change in
gene expression
NTC
siAcss2
D
NTC siAcss2
kDa
H3K18 Ac
H4K5 Bu
H3
E
i
ii
iii
Day 0
Day 7
kDa
H3K9Ac
Pan K-Bu
H3
Direct blue
H3K9 Bu
H3K23 Bu
H3K27 Bu
H4K5 Bu
H4K8 Bu
H4K12 Bu
H4
F
i
Pparg
ii
Lep
iii
Cebpd
Fold over IgG
Day 0
Day 2
Day 6
IgG
H4K5 Bu

Figure 2

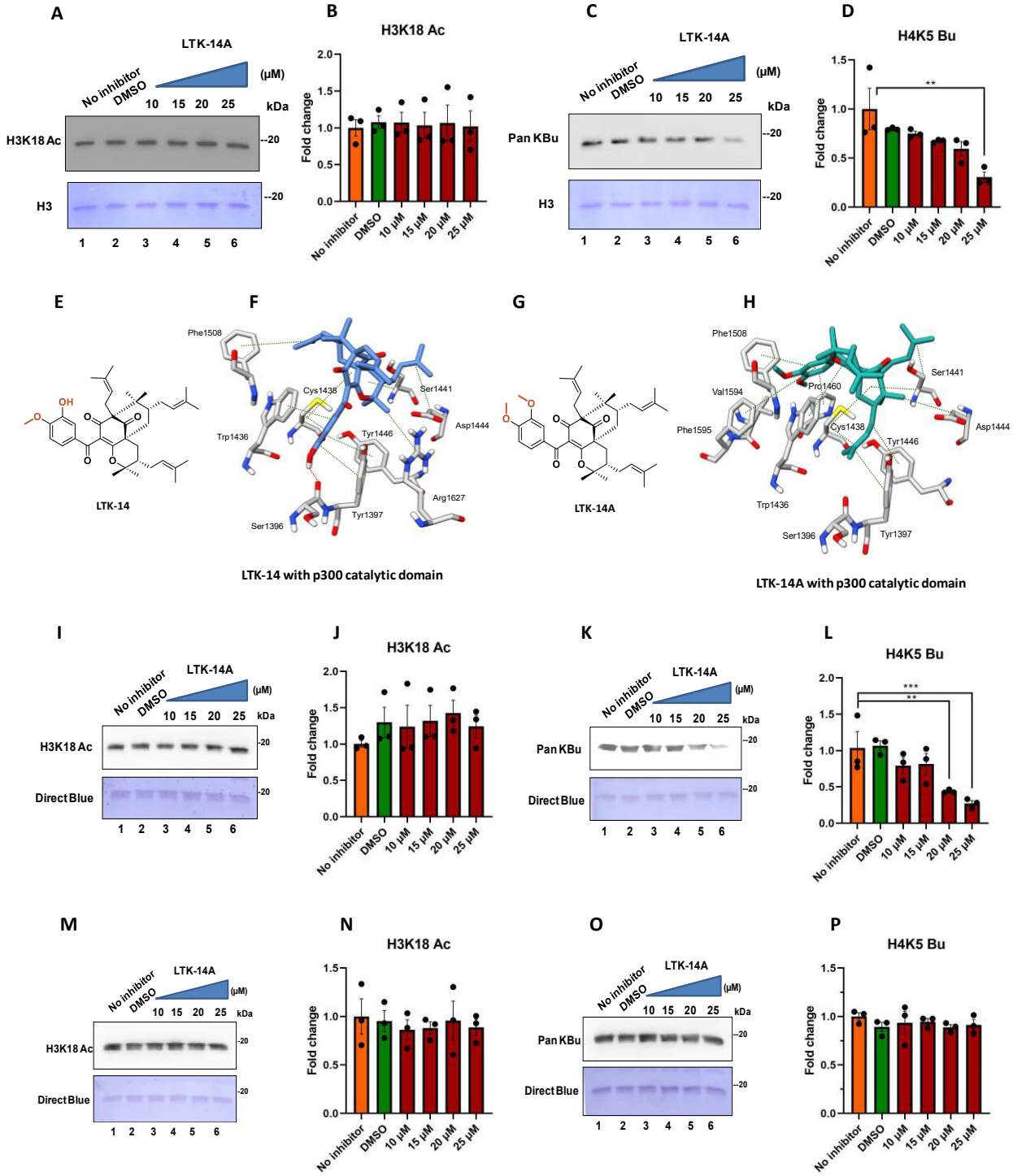
A
LTK-14A
No inhibitor
DMSO
10 15 20 25
(μM)
kDa
H3K18 Ac
H3
-20
1 2 3 4 5 6
B
H3K18 Ac
Fold change
No inhibitor
DMSO
10 μM
15 μM
20 μM
25 μM
C
LTK-14A
Pan KBu
H3
D
H4K5 Bu
**
E
OH
LTK-14
F
Phe1508
Cys1438
Ser1441
Asp1444
Trp1436
Tyr1446
Arg1627
Ser1396
Tyr1397
LTK-14 with p300 catalytic domain
G
LTK-14A
H
Phe1508
Ser1441
Val1594
Pro1460
Phe1595
Cys1438
Asp1444
Tyr1446
Trp1436
Ser1396
Tyr1397
LTK-14A with p300 catalytic domain
I
Direct Blue
J
K
L
***
**
M
N
O
P

Figure 3

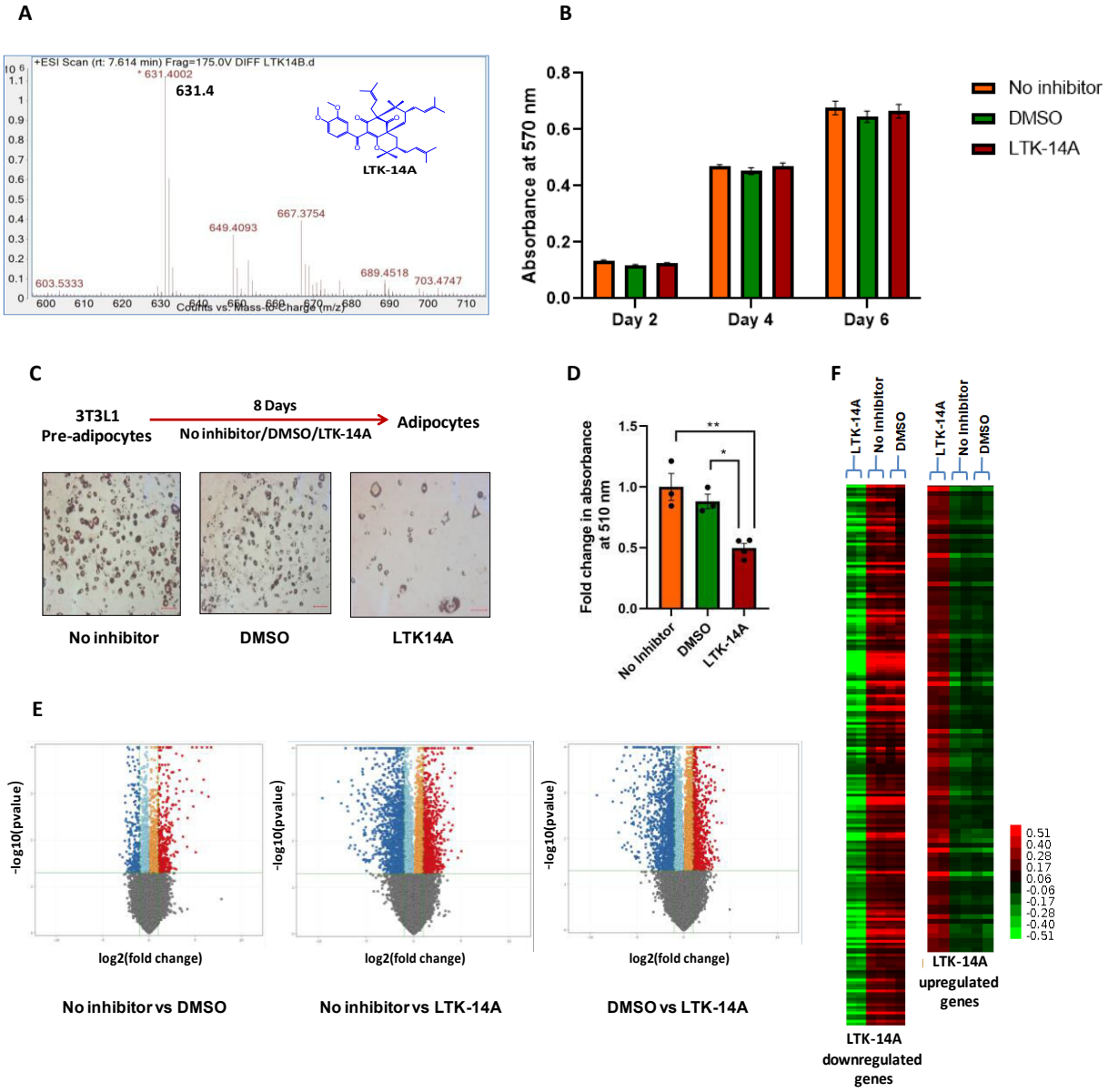
A
+ESI Scan (rt: 7.614 min) Frag=175.0V DIFF LTK14B.d
631.4
LTK-14A
667.3754
649.4093
603.5333
689.4518
703.4747
Counts vs. Mass-to-Charge (m/z)
B
Absorbance at 570 nm
Day 2
Day 4
Day 6
No inhibitor
DMSO
LTK-14A
C
3T3L1
Pre-adipocytes
8 Days
No inhibitor/DMSO/LTK-14A
Adipocytes
No inhibitor
DMSO
LTK14A
D
Fold change in absorbance at 510 nm
No Inhibitor
DMSO
LTK-14A
E
-log10(pvalue)
log2(fold change)
No inhibitor vs DMSO
No inhibitor vs LTK-14A
DMSO vs LTK-14A
F
LTK-14A
No Inhibitor
DMSO
LTK-14A upregulated genes
LTK-14A downregulated genes

Figure 4

A

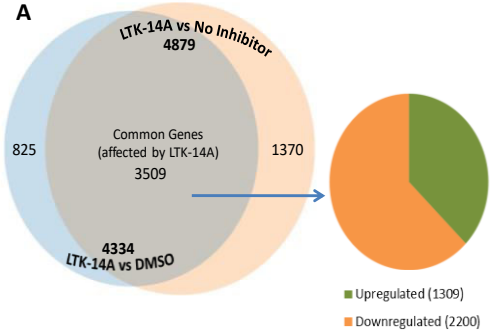

B

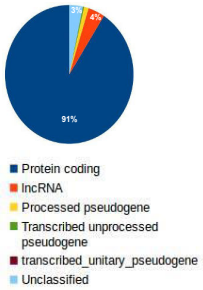

C

Biological processes	Fold enrichment	P-value	FDR
fatty acid beta-oxidation using acyl-CoA dehydrogenase	6.93	0.0000556	0.00304
positive regulation of cholesterol biosynthetic process	6.06	0.00129	0.0442
positive regulation of cholesterol metabolic process	6.06	0.00129	0.0441
positive regulation of sterol biosynthetic process	6.06	0.00129	0.044
acetyl-CoA biosynthetic process from pyruvate	6.06	0.00129	0.0439

D

Biological process	Fold enrichment	P-value	FDR
receptor localization to synapse	4.78	0.0000625	0.0448
protein localization to synapse	4.37	0.0000078	0.00724
regulation of synaptic plasticity	3.55	1.25E-09	0.00000393
signal release	2.97	0.0000189	0.0166
exocytosis	2.83	0.00000493	0.00519

E

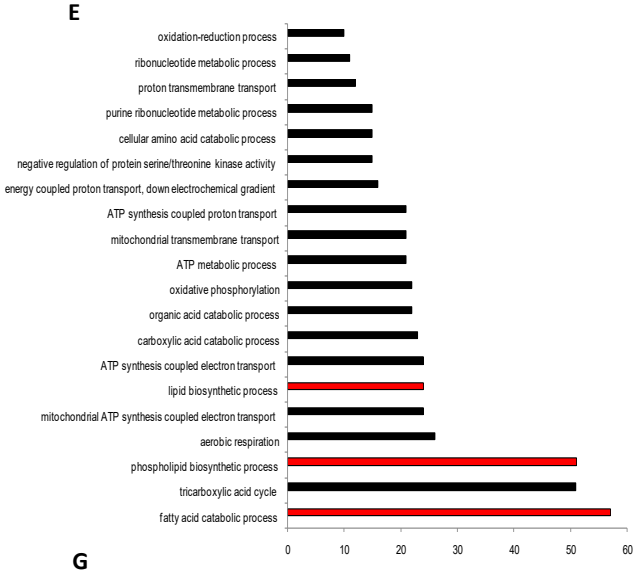

F

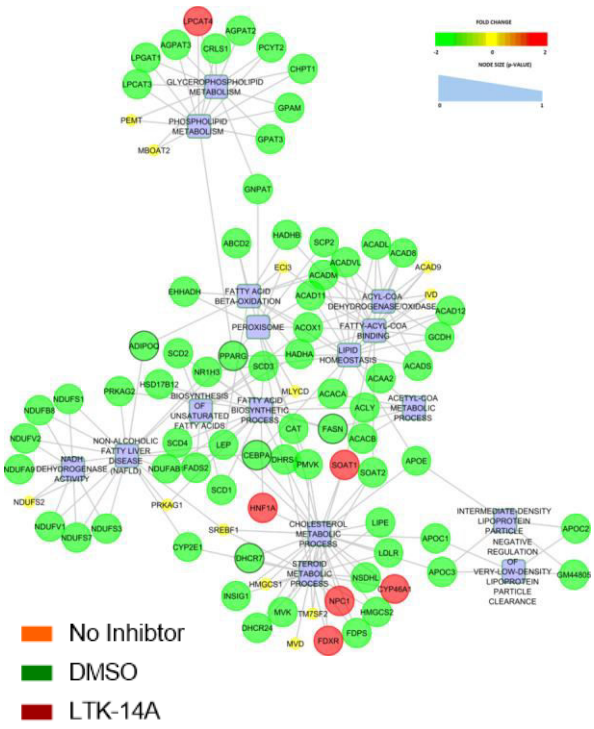

G

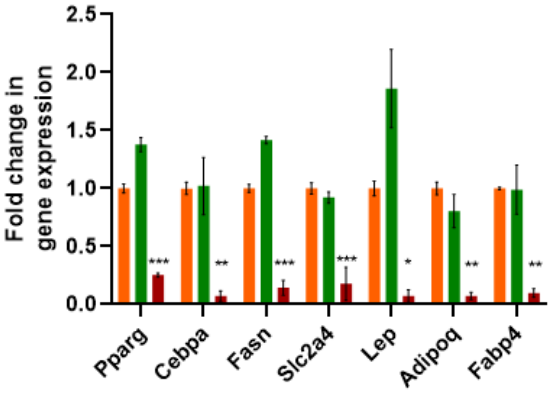

Figure 5

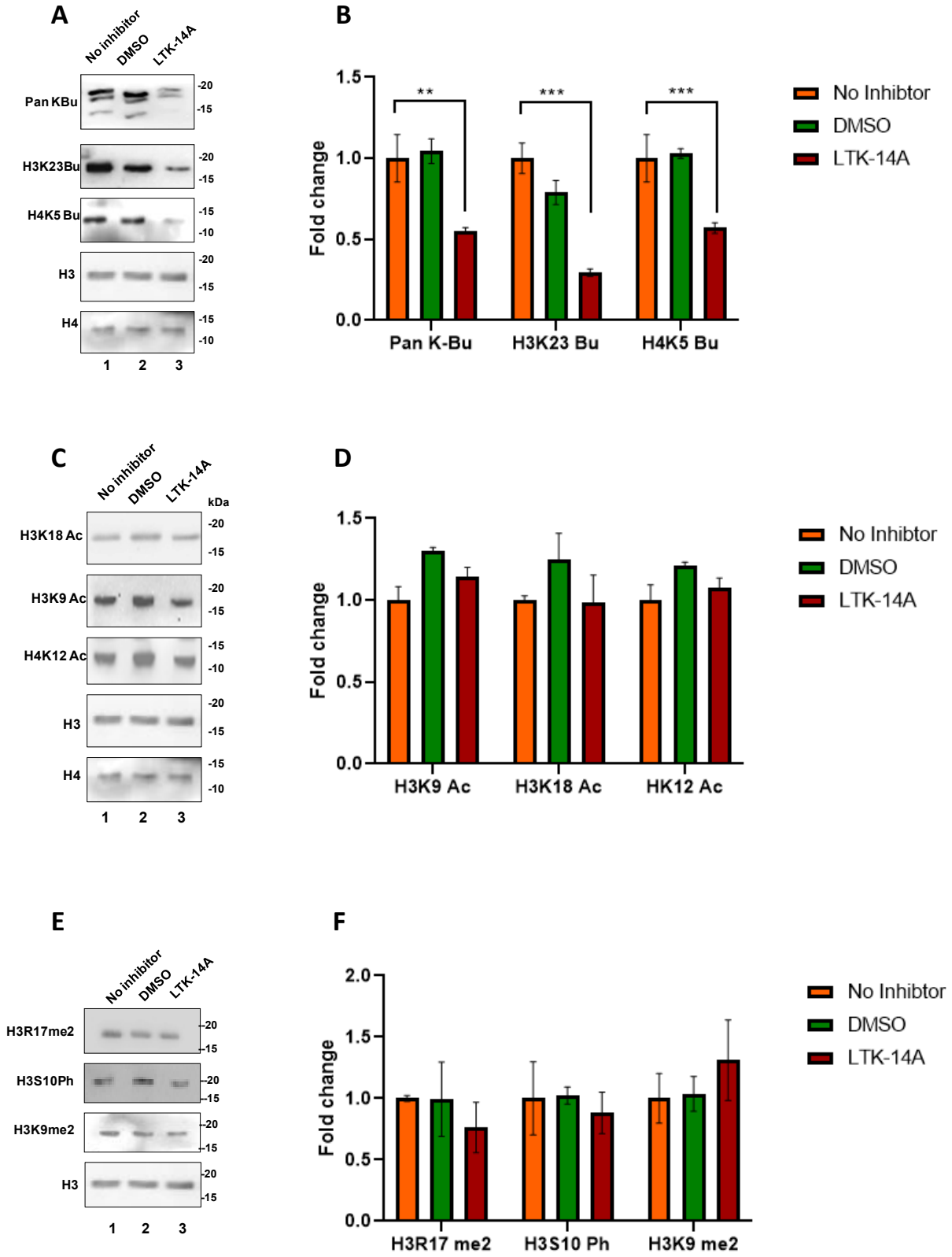
A
No inhibitor
DMSO
LTK-14A
Pan KBu
H3K23Bu
H4K5 Bu
H3
H4
-20
-15
-10
1
2
3
B
Fold change
1.5
1.0
0.5
0.0
**
***
***
Pan K-Bu
H3K23 Bu
H4K5 Bu
No Inhibtor
DMSO
LTK-14A
C
No inhibitor
DMSO
LTK-14A
kDa
H3K18 Ac
H3K9 Ac
H4K12 Ac
H3
H4
-20
-15
-10
1
2
3
D
Fold change
1.5
1.0
0.5
0.0
H3K9 Ac
H3K18 Ac
HK12 Ac
No Inhibtor
DMSO
LTK-14A
E
No inhibitor
DMSO
LTK-14A
H3R17me2
H3S10Ph
H3K9me2
H3
-20
-15
1
2
3
F
Fold change
2.0
1.5
1.0
0.5
0.0
H3R17 me2
H3S10 Ph
H3K9 me2
No Inhibtor
DMSO
LTK-14A

Figure 6

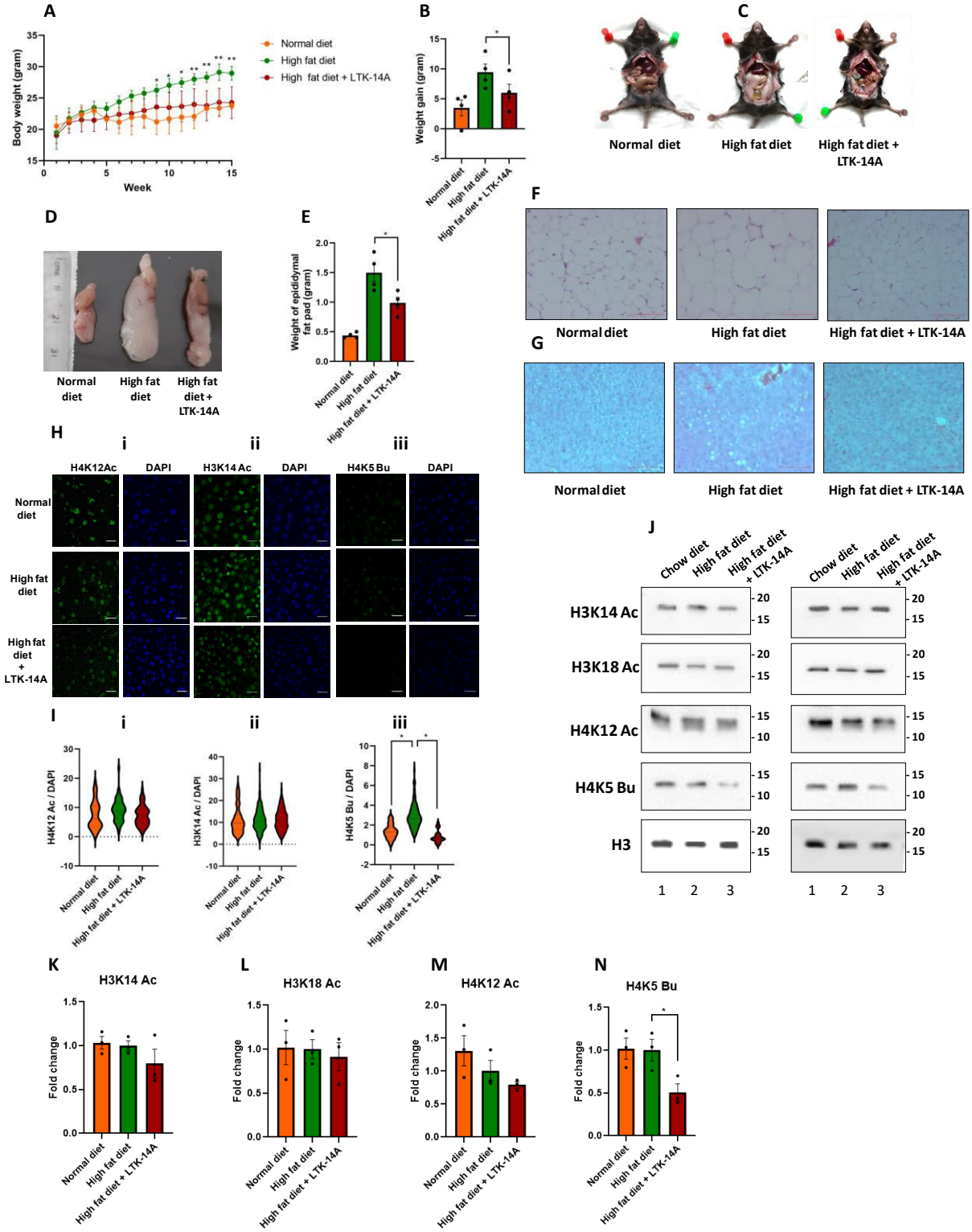
A
Body weight (gram)
Week
Normal diet
High fat diet
High fat diet + LTK-14A
B
Weight gain (gram)
Normal diet
High fat diet
High fat diet + LTK-14A
C
Normal diet
High fat diet
High fat diet + LTK-14A
D
Normal diet
High fat diet
High fat diet + LTK-14A
E
Weight of epididymal fat pad (gram)
Normal diet
High fat diet
High fat diet + LTK-14A
F
Normal diet
High fat diet
High fat diet + LTK-14A
G
Normal diet
High fat diet
High fat diet + LTK-14A
H
i
ii
iii
H4K12Ac
DAPI
H3K14 Ac
DAPI
H4K5 Bu
DAPI
Normal diet
High fat diet
High fat diet + LTK-14A
I
i
ii
iii
H4K12 Ac / DAPI
H3K14 Ac / DAPI
H4K5 Bu / DAPI
Normal diet
High fat diet
High fat diet + LTK-14A
J
Chow diet
High fat diet
High fat diet + LTK-14A
H3K14 Ac
H3K18 Ac
H4K12 Ac
H4K5 Bu
H3
1
2
3
K
H3K14 Ac
L
H3K18 Ac
M
H4K12 Ac
N
H4K5 Bu
Fold change
Normal diet
High fat diet
High fat diet + LTK-14A

Figure 7

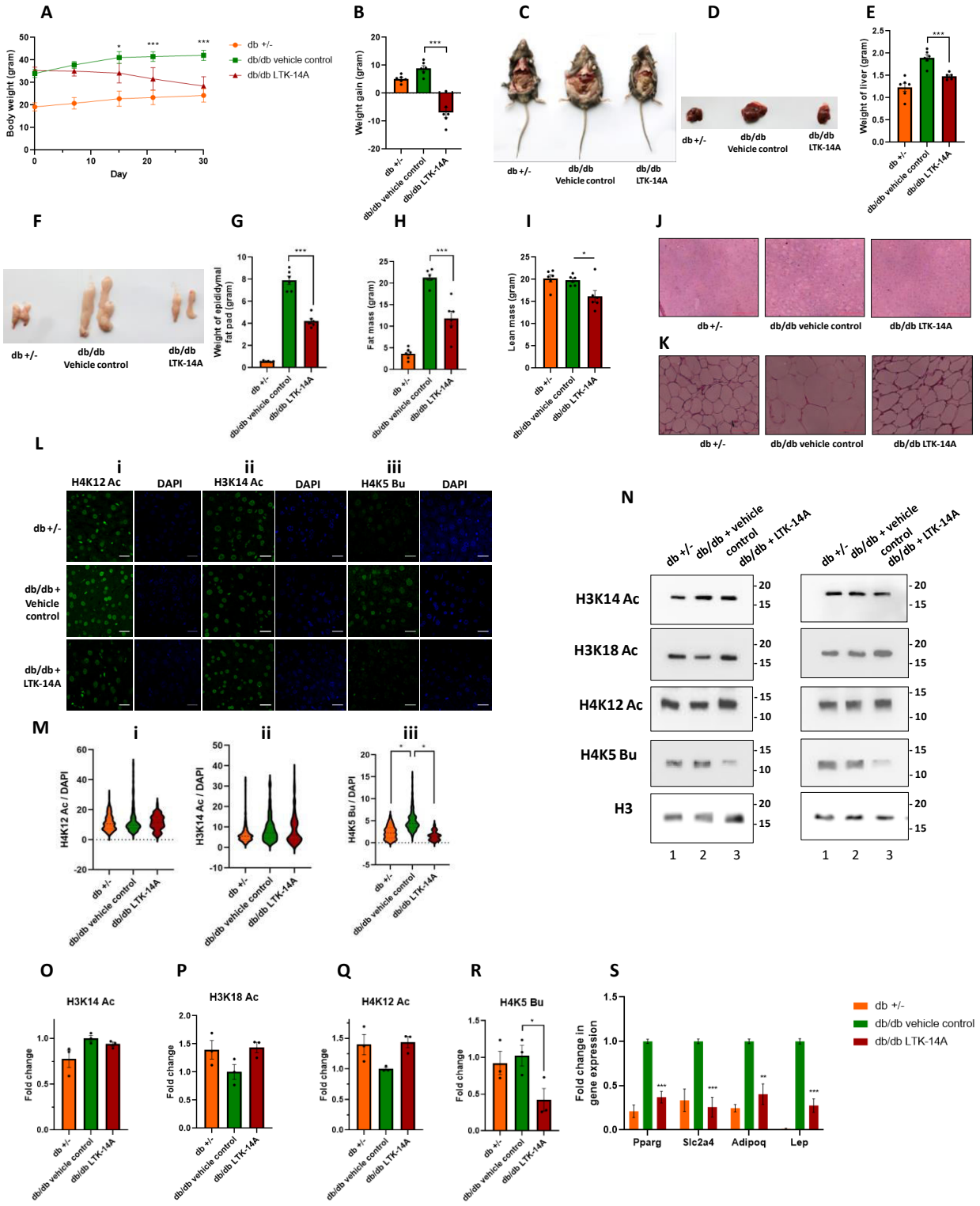
A
Body weight (gram)
Day
db +/-
db/db vehicle control
db/db LTK-14A
B
Weight gain (gram)
C
db +/-
db/db Vehicle control
db/db LTK-14A
D
E
Weight of liver (gram)
F
G
Weight of epididymal fat pad (gram)
H
Fat mass (gram)
I
Lean mass (gram)
J
K
L
i
ii
iii
H4K12 Ac
H3K14 Ac
H4K5 Bu
DAPI
db/db + Vehicle control
db/db + LTK-14A
M
H4K12 Ac / DAPI
H3K14 Ac / DAPI
H4K5 Bu / DAPI
N
db +/-
db/db + vehicle control
db/db + LTK-14A
H3K14 Ac
H3K18 Ac
H4K12 Ac
H4K5 Bu
H3
O
P
Q
R
S
Fold change
Fold change in gene expression
Pparg
Slc2a4
Adipoq
Lep
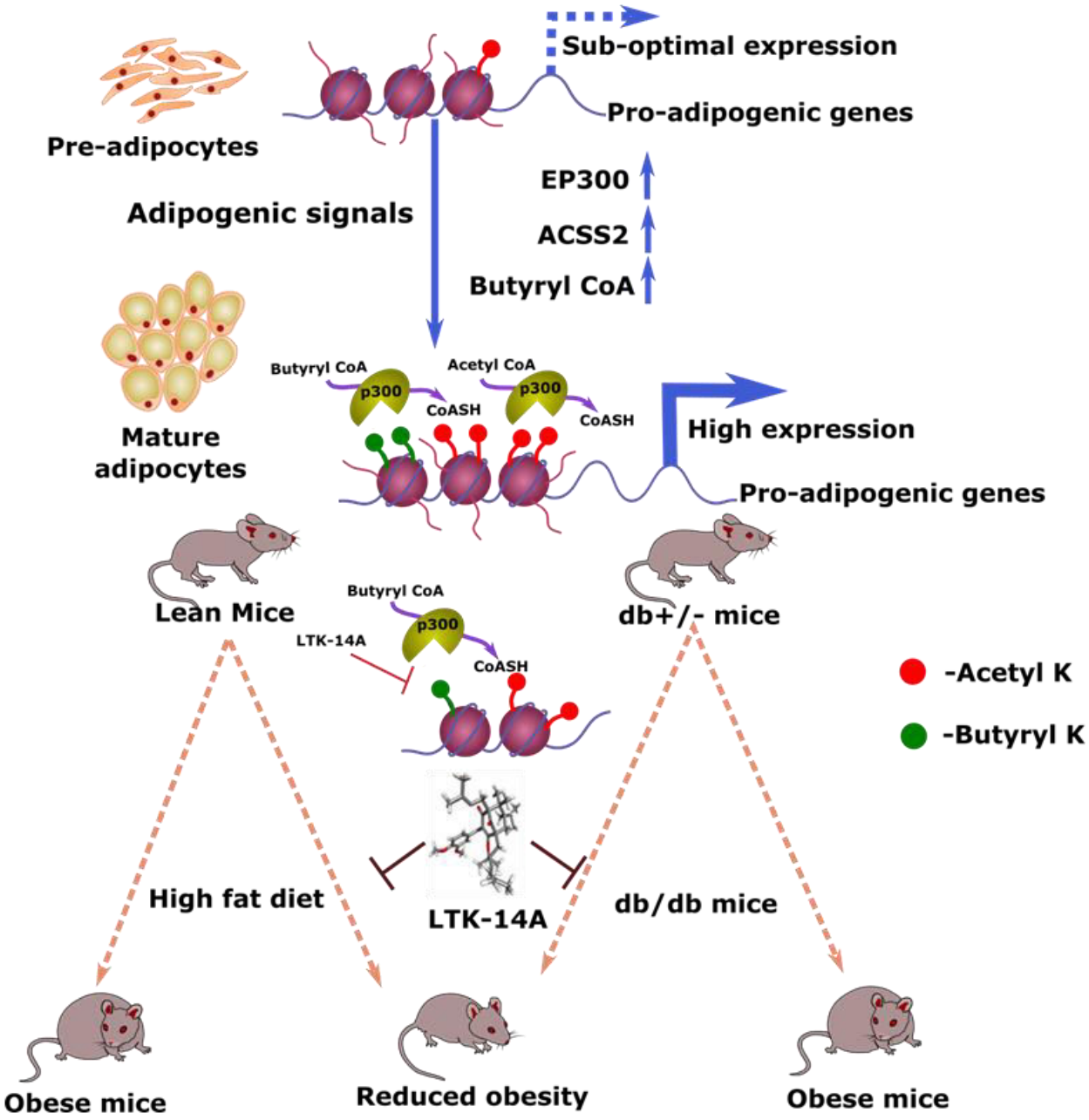
Graphical abstract